Variance Reduction for Multi-physics Analysis of Moving Systems

by

Chelsea A. D'Angelo

A dissertation submitted in partial fulfillment of
the requirements for the degree of

Doctor of Philosophy

(Nuclear Engineering and Engineering Physics)

at the

UNIVERSITY OF WISCONSIN–MADISON

2019

Date of final oral examination: 05/16/2019

The dissertation is approved by the following members of the Final Oral Committee:

Paul P. H. Wilson, Professor, Engineering Physics

Douglass Henderson, Professor, Engineering Physics

Bryan Bednarz, Professor, Medical Physics

Jake Blanchard, Professor, Engineering Physics

Andrew Davis, HPC Specialist, Culham Centre for Fusion Energy

Acknowledgments

Pursuing my PhD has been the most challenging and rewarding experience of my life. I am so thankful to have learned and grown more than I could have imagined. I certainly haven't done it alone. It takes a village to raise a grad student and I am immensely grateful for my village.

To my parents, Len and Jill, thank you for your love, support, hugs, and amazing ability to always have the right words to guide me through anything. You sparked my initial curiosity for science and engineering and provided every opportunity I needed to begin my journey into this field.

To my sister, Courtney, you are the best listener and an endless source of laughter and light. Thank you for being my cheerleader and always making the study snacks.

To my partner, Casey, thank you for always encouraging me to be brave and reach beyond my comfort zone. Through all the years of internships and grad school, thank you for helping me with everything from nuclear physics to the dishes.

To all of the CNERG members that I have overlapped with, thank you for all of the office chats, terrace outings, doughnuts, homework help, bike rides, and frisbee sessions. I couldn't have been luckier to spend my time with a more kind and inclusive research group.

To my LANL mentors, Karen and Steve, thank you for encouraging me to apply to grad school, providing real-world experience that helped me prepare, and

advocating for me when it came time to start my career.

To my UW mentor, Andy, you are a brilliant teacher and incredibly generous with your time. Thank you for the countless hours of coding and debugging support made to be way more enjoyable with the addition of British culture lessons.

To my advisor, Paul, thank you for cultivating an incredibly supportive environment, a safe space to learn and ask questions, advice on navigating through the tough moments, and most importantly, the guidance I needed to help me believe in myself.

Contents

List of Figures

Abstract

The quantification of the shutdown dose rate (SDR) caused by photons emitted by activated structural materials is an important and necessary step of the design process of fusion energy systems (FES). FES are purposefully designed with modular components that can be moved out of a facility after shutdown for maintenance. It is particularly important to accurately quantify the SDR during maintenance procedures that may cause facility personnel to be in closer proximity to activated equipment. This type of analysis requires neutron and photon transport calculations coupled by activation analysis to determine the SDR. Due to its ability to obtain highly accurate results, the Monte Carlo (MC) method is often used for both transport operations, but the computational expense of obtaining results with low error in systems with heavy shielding can be prohibitive. However, variance reduction (VR) methods can be used to optimize the computational efficiency by artificially increasing the simulation of events that will contribute to the quantity of interest.

One hybrid VR technique used to optimize the initial transport step of a multi-step process is known as the Multi-Step Consistent Adjoint Driven Importance Sampling (MS-CADIS) method. The basis of MS-CADIS is that the importance function used in each step of the problem must represent the importance of the particles to the final objective function. As the spatial configuration of the materials changes, the probability that they will contribute to the objective function also changes. In the specific case of SDR analysis, the importance function for the neutron transport step must capture the probability of materials to become activated and subsequently emit photons that will make a significant contribution to the SDR. The Groupwise Transmutation (GT)-CADIS method is an implementation of MS-CADIS that optimizes the neutron transport step of SDR calculations. GT-CADIS generates an adjoint neutron source based on

certain assumptions and approximations about the transmutation network. This source is used for adjoint transport and the resulting flux is used to generate the biasing parameters to optimize the forward neutron transport.

For systems that undergo movement, a new hybrid deterministic/MC VR technique, the Time-integrated (T)GT-CADIS method, that adapts GT-CADIS for dynamic systems by calculating a time-integrated adjoint neutron source was developed. This work demonstrates the tools and workflows necessary to efficiently calculate quantities of interest resulting from coupled, multi-physics processes in dynamic systems.

Chapter 1

Introduction

The rapid design iteration process of complex nuclear systems has long been aided by computational simulation. Traditionally, these simulations involve radiation transport in static geometries. However, in certain scenarios, it is desirable to investigate dynamic systems and the effects caused by the motion of one or more components. For example, fusion energy systems (FES) are purposefully designed with modular components that can be moved out of a facility after shutdown for maintenance purposes. To ensure the safety of maintenance personnel, it is important to accurately quantify the shutdown dose rate (SDR) caused by the photons emitted by structural materials that were activated during device operation. This type of analysis requires neutron transport to determine the neutron flux, activation analysis to determine the isotopic inventory, and finally a photon transport calculation to determine the SDR. One method for performing this analysis is known as the Rigorous 2-Step Method (R2S) because the neutron and photon transport are performed in separate calculations [1].

While Monte Carlo (MC) calculations are considered to be the most accurate method for simulating radiation transport, the computational expense of obtaining

results with low error in systems with heavy shielding can be prohibitive. However, variance reduction (VR) methods can be used to increase computational efficiency. There are many types of VR methods that revolve around the basic theory of artificially increasing the simulation of events that will contribute to the quantity of interest, such as flux or dose rate. One class of VR techniques takes advantage of the speed of deterministic codes to provide an estimate of the adjoint solution of the transport equation to automatically generate biasing parameters to accelerate the MC transport. The adjoint flux has significance as a measure of the importance of a region of phase space to the objective function.

One hybrid VR technique used to optimize the initial transport step of a multi-step process is known as the Multi-Step Consistent Adjoint Driven Importance Sampling (MS-CADIS) [2]. The basis of MS-CADIS is that the importance (adjoint) function used in each step of the problem must represent the importance of the particles to the final objective function. In the specific case of SDR calculations, the importance function for the neutron transport step must capture the probability of materials to become activated and subsequently emit photons that will make a significant contribution to the SDR. The Groupwise Transmutation (GT)-CADIS method is an implementation of MS-CADIS that optimizes the neutron transport step of SDR calculations [3]. GT-CADIS generates an adjoint neutron source based on certain assumptions and approximations about the transmutation network. This source is used for adjoint neutron transport and the resulting adjoint flux is used to generate the biasing parameters to optimize the forward neutron transport. For cases involving coupled multi-physics analysis in dynamics systems, such as SDR calculations during maintenance activities, a new hybrid deterministic/MC VR technique that adapts GT-CADIS for dynamic systems by calculating a time-integrated adjoint neutron source was developed.

The goal of this work is to develop the workflow and tools necessary to efficiently calculate quantities of interest resulting from coupled, multi-physics processes in dynamic systems. The main application is the quantification of the SDR resulting from the coupled neutron irradiation-photon emission that occurs in FES; specifically investigating how to optimize the SDR calculation when activated system components are moved during maintenance activities. A tool was developed to implement rigid-body transformations on the CAD-based geometry and the R2S and GT-CADIS methods were adapted to incorporate dynamics. An experiment was contrived to demonstrate the limitations of existing VR methods as they apply to dynamic problems and verify the efficacy of this new method. Given these objectives, Chapter 2 will include background and theory relevant to VR methods in coupled, multi-physics systems. It begins with an introduction to computational radiation transport, specifically the Monte Carlo method. Next, Chapter 4 shows the experiment demonstrating the need for a new VR method to optimize the SDR in dynamic systems. Chapter 3 discusses the implementation and gives a demonstration of the time-integrated (T)R2S method. The derivation of the time-integrated (T)GT-CADIS VR parameters that will optimize the SDR in dynamic systems is given in Chapter 5. The implementation plan and a demonstration of this method are also given in this chapter. Finally, Chapter 6 shows a production-level demonstration of the TGT-CADIS and TR2S methods using the Spherical Tokamak Fusion Nuclear Science Facility ST-FNSF device.

Chapter 2

Literature Review

The goal of this work is to optimize the initial radiation transport step of a coupled, multi-physics process occurring in a system that has moving components. One important application of this work is the quantification of the shutdown dose rate (SDR) during maintenance operations in fusion energy systems (FES).

During the operation of a fusion energy device, the nuclear reactions (e.g. D-T fusion) occurring in the plasma result in the production of high energy (14 MeV) neutrons that penetrate deeply into the system components. Some of the neutron reaction pathways result in the production of radioisotopes that persist long after device shutdown. The activated components emit high energy photons as they reach stability over time. These high energy photons can cause grave health effects, therefore it is necessary to quantify the dose rate in order to ensure the safety of personnel working in fusion facilities. This is not only important for the time during operation and immediately after shutdown when the device is in a static configuration, but also during maintenance activities when the dose rate at a point changes over time as a function of the position of the activated components.

Performing computational simulations of the radiation transport in these devices

and calculating quantities of interest, such as flux and dose rate, are a crucial part of the fusion reactor design phase. These simulations can inform decisions about the sustainability and safety of the device. This chapter will provide background on computational radiation transport, methods for SDR analysis, methods for optimizing radiation transport calculations, and finally how radiation transport calculations are currently handled in systems with moving geometries and sources.

2.1 Analog Monte Carlo Calculations

Computational analysis of nuclear systems is most often performed by either deterministic or stochastic codes. Deterministic codes discretize the problem in space, energy, and direction in order to obtain an approximate solution to the Boltzmann transport equation. Obtaining high fidelity solutions in every region of phase space requires increasing the discretization which can become very memory intensive for large problems. The Monte Carlo (MC) method is a stochastic solution to the transport equation [4] that involves the simulation of random particle walks through phase space. Achieving high fidelity results with the MC method does not have the same prohibitively high memory requirements for large, complex problems. Therefore, the most optimal way to obtain accurate particle distributions in FES is through MC radiation transport.

When the analog operation mode (i.e. no variance reduction) of MC analysis is used to solve radiation transport calculations, the source particle's position, energy, direction, and subsequent collisions are sampled from unbiased probability distribution functions (PDFs) that describe physical particle behavior. The particle's journey through space, or its history, is tracked until it is terminated. Quantities of interest such as flux can be scored, or tallied, by averaging particle tracks in discrete

regions of phase space.

One challenge incurred by MC simulations of FES is the presence of heavily shielded regions. The particles undergo many collisions (absorption and scattering) in the shielding which results in low particle fluxes in the attenuated regions. Regions that have low particle fluxes are sampled less frequently and therefore have higher statistical uncertainty than regions with high flux that are sampled very often.

This uncertainty can be represented by the relative error, $\mathfrak{R}$, which is defined by Eq. 2.1:

$$\mathfrak{R} = \frac{\sigma_{\overline{x}}}{\overline{x}} \tag{2.1}$$

where $\overline{x}$ is the mean of the tally scores and $\sigma_{\overline{x}}$ is the standard deviation of the mean.

For a well behaved, properly converged tally, $\sigma_{\overline{x}}$ is proportional to $1/\sqrt{N}$ where N is the number of histories [5]. Therefore, to reduce the uncertainty, one can increase the number of particle histories simulated. Compute time scales linearly with N, and $\mathfrak{R}$ is inversely proportional to $\sqrt{N}$, therefore to reduce the error by half, the number of histories, and therefore time, required will quadruple.

The efficiency of MC calculations is measured by a quantity known as the figure of merit (FOM). The FOM is a function of relative error, $\mathfrak{R}$, and computer processing time, t_{proc}:

$$\text{FOM} = \frac{1}{\mathfrak{R}^2 t_{proc}}. \tag{2.2}$$

A high FOM is desirable because it means that less computation time is needed to achieve a reasonably low error (<0.1) [5].

2.2 Shutdown Dose Rate Analysis

This section will discuss the two primary workflows used to investigate the SDR: the Direct 1-Step (D1S) [6] and the Rigorous 2-Step (R2S) [1] method. Both methods couple the neutron and photon transport via activation analysis to calculate the SDR.

2.2.1 D1S

As its name implies, the D1S method performs coupled neutron-photon transport in a single simulation. It relies upon a version of the Monte Carlo N-Particle (MCNP) transport code [5] that has slight modifications as well as special cross-section data that replaces prompt gammas with decay gammas. When a prompt photon reaction is sampled in a standard MCNP simulation, the photon is stored until the original neutron transport is completed. Then, the photon is transported as part of the same simulation. The version of MCNP5 used by D1S allows the delayed photons to be emitted as if they were prompt so they can be transported in the same simulation as the neutrons. A time correction factor calculated with FISPACT [7] is later applied.

The Advanced D1S [8] includes improvements to allow for the calculation of dose rate on a 3D mesh. Because both neutron and photon transport occur in the same simulation, therefore on the same geometry, D1S is not currently applicable to geometries that undergo movement after shutdown. This has been identified as a necessary improvement and the development of a subroutine to produce portable decay photon sources for pure photon calculations is underway [8].

2.2.2 R2S

In contrast to D1S, the R2S method relies upon separate MC neutron and photon transport simulations. The transport steps are coupled through activation analysis by a nuclear inventory code. The goal of the neutron transport step is to determine the neutron flux as a function of space and energy. This neutron flux along with a specific irradiation and decay scenario are used as input into a nuclear inventory code to determine the photon emission density as a function of decay time. The calculated photon emission density for each decay time is then used as the source for MC photon transport. A photon flux tally fitted with flux-to-dose-rate conversion factors is used to determine the final SDR [1]. Because the neutron and photon transport are performed separately, different geometries can be used for each transport step which is key for simulating geometry movement after shutdown.

2.2.2.1 Mesh-based R2S

In order to calculate an accurate dose rate, it is necessary to obtain detailed distributions of the neutron flux and photon source throughout the geometry. The Mesh-tally Coupled R2S (MCR2S) tool was the first implementation of a mesh-based R2S methodology [9]. It couples MCNP neutron and photon transport calculations with the FISPACT nuclear inventory code. First, multi-group neutron fluxes are scored on a 3D mesh. Then, the geometry used for MC transport is discretized onto a mesh, a requirement of activation codes. Using the mesh-based geometry/material description, multi-group neutron fluxes, and an irradiation and decay scenario, the inventory code calculates the photon emission density in each mesh element for each decay time [9]. These photon emission density distributions are then used as sources for MC photon transport simulations.

The Python for Nuclear Engineering (PyNE) tookit has many useful functions and scripts to assist in nuclear analysis [10]. PyNE has an R2S module [11] that includes functions and scripts to implement a mesh-based R2S method for CAD geometries. The Direct Accelerated Geometry Monte Carlo (DAGMC) toolkit combined with a Monte Carlo code, such as MCNP, is used to perform radiation transport directly on the CAD geometry and score results on a mesh.

After neutron transport is performed, the material-laden geometry and mesh-based, energy-wise neutron flux tally along with irradiation and decay information are given as input to the PyNE R2S script to produce an input file for activation analysis. This analysis is performed with the Analytic and Laplacian Adaptive Radioactivity Analysis (ALARA) code [12] and a mesh-based photon source is generated for each decay time of interest.

MCNP is compiled with a custom source sampling subroutine and the mesh-based photon source is used as a source for photon transport. Photon flux tallies fitted with flux-to-dose rate conversion factors are used to calculate the SDR at each decay time.

2.3 Monte Carlo Variance Reduction Methods

As mentioned in section 2.1, the presence of highly attenuating structural materials in FES presents a challenge for MC calculations. Regions with low particle fluxes are not sampled as frequently and therefore have higher statistical uncertainty associated with results scored there. A set of techniques, known as variance reduction (VR), can be used to decrease the statistical uncertainty in these results in a more efficient way than the brute force method of increasing the number of particle histories. VR methods aim to increase the FOM, a measure of efficiency given in Eq. 2.2, by

reducing the compute time necessary to achieve a statistically reasonable result. This is done by modifying particle behavior to preferentially sample trajectories that are likely to contribute to the tallies of interest.

One way this is accomplished is by sampling from biased PDFs instead of the standard PDFs used in analog calculations that describe actual particle behavior. In order to compensate for this biased sampling, the particle statistical weight is adjusted [13]. The relationship between the particle statistical weight, w, and the PDF that governs particle behavior is given in Eq. 2.3:

$$w_{\text{biased}}\text{pdf}_{\text{biased}} = w_{\text{unbiased}}\text{pdf}_{\text{unbiased}}. \tag{2.3}$$

If the biased sampling results in an event occurring more frequently than it does in reality, the particle weight is decreased and vice verse. Using biased PDFs to preferentially sample events that will result in an increased number of histories that contribute to the tally of interest can decrease the standard deviation, and therefore relative error, $\mathfrak{R}$, which will increase the FOM.

Another method of VR is particle splitting and rouletting. To increase the number of particle histories that can contribute to a tally of interest, it is desirable to split particles as they enter more important regions and roulette particles as they enter less important regions. The decision to split or roulette particles first requires assigning an importance, I, to every region in the geometry. When a particle moves from a region A to a region B, the ratio of importances is calculated. If region B is more important than region A such that $I_B/I_A \geqslant 1$, the particle with original weight w_0 is split into $n = I_B/I_A$ particles, each with weight w_0/n. If instead region B is less important than region A such that $I_B/I_A < 1$, the particle will undergo roulette. The particle will survive with a probability n and weight w_0/n [14]. This is particularly

useful in calculating results in heavily attenuated regions, like in FES. Importances can be assigned in a way that will force particle flow towards the region of interest.

The weight window method in the Monte Carlo N-Particle (MCNP) code is a flow control method that utilizes particle splitting and rouletting. A weight window is a region of phase-space that is assigned an upper and lower bound on the particle's weight. The windows can be assigned to cells in the geometry or on a superimposed mesh and to energy bins. When a particle enters a weight window, its weight is assessed; if its weight is above the upper bound, it is split and if it is below the lower bound, it is rouletted.

The manual generation of weight window bounds requires a priori knowledge of the problem physics and becomes increasingly difficult with the complexity of the geometry. Historically, this process has required a considerable amount of time and effort of a skilled analyst, but there are now various methods to produce these weight window bounds automatically. Some of these methods will be discussed in the following section.

2.4 Automated Variance Reduction

Many techniques have been developed over the years to automate the selection and assignment of modified sampling and weight control parameters to reduce computational and human effort.

One class of VR techniques, known as hybrid deterministic/MC methods, takes advantage of the speed of deterministic transport to estimate a solution to the adjoint Boltzmann transport equation which can then be used to generate MC VR parameters. The adjoint solution has significance as a measure of importance of a particle to some specified objective function.

To demonstrate the use of the adjoint solution as an importance function, first start with the operator form of the linear, time-independent Boltzmann transport equation [4]:

$$H\Psi(\vec{r}, E, \widehat{\Omega}) = q(\vec{r}, E, \widehat{\Omega}). \tag{2.4}$$

Ψ is the angular flux, q is the source of particles, and the operator H which describes all particle behavior is given by:

$$H = \widehat{\Omega} \cdot \nabla + \sigma_t(\vec{r}, E) - \int_0^\infty dE' \int_{4\pi} d\Omega' \sigma_s(\vec{r}, E' \to E, \widehat{\Omega}' \to \widehat{\Omega}) \tag{2.5}$$

where σ_t is the total cross-section and σ_s is the double-differential scattering cross-section. The source and angular flux are functions of six independent variables: a three-dimensional position vector ($\vec{r}$) a two-dimensional directional vector ($\widehat{\Omega}$), and energy (E). The adjoint identity is stated in Eq. 2.6 as:

$$\langle \Psi^+, H\Psi \rangle = \langle \Psi, H^+\Psi^+ \rangle \tag{2.6}$$

where $\langle \cdot \rangle$ refers to the integration over space, energy, and angle and the adjoint operator H^+ is given by:

$$H^+ = -\widehat{\Omega} \cdot \nabla + \sigma_t(\vec{r}, E) - \int_0^\infty dE' \int_{4\pi} d\Omega' \sigma_s(\vec{r}, E \to E', \widehat{\Omega} \to \widehat{\Omega}'). \tag{2.7}$$

This identity can be used to form the adjoint transport equation:

$$H^+\Psi^+ = q^+. \tag{2.8}$$

Substituting Eq.2.4 and 2.8 into Eq. 2.6, the adjoint identity can also be written

as:

$$\langle \Psi^+, q \rangle = \langle \Psi, q^+ \rangle. \tag{2.9}$$

As mentioned, the solution to the adjoint transport equation will be used as an importance function therefore the thoughtful selection of an adjoint source q^+ is needed.

Consider the equation for detector response, R:

$$R = \langle \Psi, \sigma_d \rangle \tag{2.10}$$

where σ_d is a detector response function. If the adjoint source is chosen to be equivalent to the detector response function:

$$q^+ = \sigma_d \tag{2.11}$$

and substituted into Eq. 2.10:

$$R = \langle \Psi, q^+ \rangle \tag{2.12}$$

the response has the same form as the right side of Eq. 2.9. Therefore, the response can also be written as a function of the adjoint solution:

$$R = \langle \Psi^+, q \rangle. \tag{2.13}$$

This final relation allows us to know the response R for any source q once the adjoint solution Ψ^+ to a quantity of interest is known.

2.4.1 CADIS

The Consistent Adjoint Driven Importance Sampling (CADIS) method is one of the hybrid deterministic/MC VR techniques that uses the adjoint solution as an importance function to formulate VR parameters for MC transport [13]. More specifically, CADIS provides a method for generating a biased source and the weight window lower bounds in a consistent manner. The consistent generation of biasing parameters ensures that particles are born within weight windows, eliminating any loss of efficiency due to particle splitting/rouletting immediately after birth.

Recall that the response, or tally, of interest in a transport calculation can be represented in terms of the adjoint flux by Eq. 2.13. To decrease the variance, the CADIS method formulates a biased source distribution, $\widehat{q}$, that represents the contribution of particles from phase space $(\vec{r}, E, \widehat{\Omega})$ to the total detector response, R:

$$\widehat{q}(\vec{r}, E, \widehat{\Omega}) = \frac{\Psi^{+}(\vec{r}, E, \widehat{\Omega}) q(\vec{r}, E, \widehat{\Omega})}{R}. \tag{2.14}$$

This is a way to bias the sampling of source particles as a function of their contribution to the total detector response.

As previously mentioned, when sampling from a biased distribution, the particle weight needs to be adjusted such that total weight is conserved in order to eliminate systematic bias:

$$w(\vec{r}, E, \widehat{\Omega}) \widehat{q}(\vec{r}, E, \widehat{\Omega}) = w_0 q(\vec{r}, E, \widehat{\Omega}). \tag{2.15}$$

Substituting Eq. 2.14 into Eq. 2.15 and setting w_0 equal to one, the corrected particle weight is given by:

$$w(\vec{r}, E, \widehat{\Omega}) = \frac{R}{\Psi^{+}(\vec{r}, E, \widehat{\Omega})}. \tag{2.16}$$

The corrected particle weight has an inverse relation to the adjoint flux, or importance

function. This means regions that have a high adjoint flux will have lower weight window lower bounds, meaning particles will be split.

The width of the weight windows is determined by a parameter defined to be the ratio between upper and lower bounds $\alpha = w_u/w_l$. MCNP uses a default value of $\alpha = 5$. The equation for weight window lower bounds is given by:

$$w_l(\vec{r}, E, \widehat{\Omega}) = \frac{R}{\Psi^+(\vec{r}, E, \widehat{\Omega})(\frac{\alpha+1}{2})}. \tag{2.17}$$

CADIS is ideally suited to reduce the variance of a detector response in a single target because the source chosen for adjoint transport is the detector response function corresponding to the detector of interest. There are other methods, such as FW-CADIS, that are suited for reducing the variance in multiple targets or even globally.

2.4.2 FW-CADIS

The Forward-Weighted (FW)-CADIS method is another hybrid deterministic/MC VR method. FW-CADIS aims to increase the efficiency of detector responses globally or in multiple localized targets [15]. The goal is to create uniform particle density in the tally regions thereby creating uniform statistical uncertainty in the MC results. This method relies upon a forward deterministic transport solution to weight the source for adjoint deterministic transport. The adjoint solution is then used with the standard CADIS method to produce source and transport biasing parameters for the forward MC transport simulation.

If the objective is a spatially dependent total response rate throughout the prob-

lem domain, the FW-CADIS adjoint source is formulated as:

$$q^{+}(\vec{r}, E) = \frac{\sigma_d(\vec{r}, E)}{\int_E \phi(\vec{r}, E)\sigma_d(\vec{r}, E)dE} \tag{2.18}$$

where $\sigma_d(\vec{r}, E)$ is the response function. This effectively weights the adjoint source by the inverse of the total forward response which means that in regions with low forward flux, the adjoint flux, and therefore importance, will be high and vice verse. This will result in the overall goal of nearly equal statistical uncertainty in regions of interest.

2.5 Automated Variance Reduction for Multi-physics Analysis

In its essence, SDR analysis is the analysis of a coupled, multi-physics system; the initial neutron irradiation is coupled to the decay photon transport through activation analysis. As discussed in section 2.2.2, the R2S method requires separate MC calculations for the neutron and photon transport. If the MC steps are performed in analog, applying the R2S workflow to full-scale, 3D FES becomes impractical due to the computational effort required to produce accurate space- and energy-dependent fluxes throughout the geometry.

Optimizing the final step, photon transport in the case of SDR analysis, can be done through a straightforward application of the CADIS method to solve for the response at a single detector or the FW-CADIS method if the response is desired in multiple detectors or globally.

Optimizing the initial step of a multi-step process, neutron transport in the case of SDR, is not as straightforward. The Multi-Step CADIS method described in the

next section provides an explanation for this challenge and a method for solving it.

2.5.1 MS-CADIS

The Multi-Step (MS)-CADIS method of VR was developed to optimize the primary radiation transport in a coupled, multi-step process.

Optimizing the initial radiation transport relies upon the use of a function that represents the importance of the particles to the final response of interest, not the response of that individual step [2]. This is challenging because the the final response of interest depends on the subsequent steps of the multi-step process.

MS-CADIS can be applied to any coupled, multi-step process. This will be discussed in more detail in Section 5.1. When it is applied to SDR calculations, it aims to increase the efficiency of the neutron transport step using an importance function that captures both the potential of regions to become activated and their potential to produce decay photons that contribute to the final SDR [2].

The importance function represents the expected contribution from a particle at some point in phase space to the detector response. The detector response can be expressed as the inner product of the importance function, I, and the source distribution, q:

$$R = \langle I(\vec{r}, E), q(\vec{r}, E) \rangle. \tag{2.19}$$

MS-CADIS provides a method to calculate an approximation of this importance function where the response is the final response of the multi-step process. In the case of an R2S calculation, the final response is the SDR caused by the decay photons. The SDR is defined as

$$SDR = \langle \sigma_d(\vec{r}, E_\gamma), \phi_\gamma(\vec{r}, E_\gamma) \rangle \tag{2.20}$$

where σ_d is the flux-to-dose-rate conversion factor at the position of the detector and ϕ_γ is photon flux. Following the CADIS method, the adjoint photon source is chosen to be σ_d, so the equation for SDR becomes:

$$SDR = \langle q_\gamma^+(\vec{r}, E_\gamma), \phi_\gamma(\vec{r}, E_\gamma)\rangle. \tag{2.21}$$

From the adjoint identity, Eq. 2.9, the SDR can also be written as:

$$SDR = \langle q_\gamma(\vec{r}, E_\gamma), \phi_\gamma^+(\vec{r}, E_\gamma)\rangle \tag{2.22}$$

which has the same form as Eq. 2.19. Therefore, it can be seen that the adjoint flux, ϕ_γ^+, is an importance function.

Because the final goal is to formulate a function that represents the importance of neutrons the final SDR, the neutron response is set equal to the photon response:

$$SDR = \langle q_n^+\vec{r}, E_n), \phi_n(\vec{r}, E_n)\rangle = \langle q_n\vec{r}, E_n), \phi_n^+(\vec{r}, E_n)\rangle. \tag{2.23}$$

It can be seen that the far right side of Eq. 2.23 also has the same form as Eq. 2.19 which means that the adjoint neutron flux, ϕ_n^+, serves as an importance function.

Combining equations 2.22 and 2.23, gives the relationship between the neutron and photon responses:

$$\langle q_n^+(\vec{r}, E_n), \phi_n(\vec{r}, E_n)\rangle = \langle q_\gamma(\vec{r}, E_\gamma), \phi_\gamma^+(\vec{r}, E_\gamma)\rangle. \tag{2.24}$$

To generate the adjoint neutron flux, an adjoint neutron source, q_n^+, first needs to be formulated. This requires Eq. 2.24 and another equation relating the photon source, q_γ, to the neutron flux, ϕ_n. The solution method for the adjoint neutron

source, q_n^+, will be discussed in the next section.

2.5.2 GT-CADIS

The Groupwise Transmutation (GT)-CADIS method is an implementation of MS-CADIS solely for SDR analysis. It provides a solution to the adjoint neutron source, q_n^+, by calculating a coupling term that relates the neutron flux to the photon source [3].

Neutron activation is the cause of the photon decay source so the photon source at a single point can be expressed as a non-linear function of ϕ_n:

$$q_\gamma(E_\gamma) = \int_{E_n} f(\phi_n) dE_n. \tag{2.25}$$

This function can not be linearized for arbitrary transmutation networks and irradiation scenarios, but a linear approximation can be formulated when a set of criteria, known as the Single Neutron Interaction Low Burnup (SNILB) criteria, are met [3]. When met, a solution for the coupling term, $T(\vec{r}, E_n, E_\gamma)$, which approximates the transmutation process and is defined by equation Eq. 2.26:

$$q_\gamma(\vec{r}, E_\gamma) = \int_{E_n} T(\vec{r}, E_n, E_\gamma)\phi_n(\vec{r}, E_n) dE_n \tag{2.26}$$

can be found. Equation 2.26 can then be substituted into Eq. 2.24 in order to solve for the adjoint neutron source:

$$q_n^+(\vec{r}, E_n) = \int_{E_\gamma} T(\vec{r}, E_n, E_\gamma)\phi_\gamma^+(\vec{r}, E_\gamma) dE_\gamma. \tag{2.27}$$

To calculate T, a series of single energy group neutron irradiations is performed

on each material in the geometry. The irradiation of the material in volume element v, by a flux of neutrons in energy group g, to the corresponding source of photons in energy group h, at decay time dt, is given by Eq. 2.28:

$$T_{v,g,h,dt} = \frac{q_{\gamma,v,h,dt}(\phi_{n,v,g})}{\phi_{n,v,g}}. \tag{2.28}$$

It has been shown that for typical FES spectra, materials, and irradiation scenarios, the SNILB criteria are met [3]; therefore, GT-CADIS provides a solution for T, and therefore the adjoint neutron source needed to optimize the neutron transport step of SDR analysis of FES.

2.6 Moving Geometries and Sources

2.6.1 MCNP6 Moving Objects Capability

Historically, MC analysis of moving systems was performed using a series of separate simulations with different input files that contained step-wise changes of the geometry configuration. The new moving object capability that will be available in a future version of MCNP6 allows for the motion of objects, sources, and delayed particles during a single simulation [16], [17]. This capability allows for rigid body transformations of objects including rectilinear translations and curvilinear translations and rotations. The objects can move with constant velocity, constant acceleration, or be relocated. Object kinetics are not treated, however, so the user must use caution and supply transformations that will not cause objects to overlap. This capability is currently applicable to MCNP's native geometry format, constructive solid geometry (CSG), and is not available for mesh-based geometries.

Sources can be assigned to moving objects, and therefore can move with the

same dynamics as other objects in the problem. This capability also allows for the treatment of secondary particles emitted by objects in motion. This treatment is only approximate because the geometry is fixed during the transport of source or delayed particles. This is a valid approximation due to the assumption that in most cases, the geometry movement is orders of magnitude slower than particle transport.

During the MCNP simulation, source particles are tracked through the geometry from the time of emission to termination. If any of the source particle's interactions result in the creation of a prompt or delayed secondary particle, that information is stored. After the source particle has terminated, any stored secondary particles are retrieved and transported. In the case of delayed particles emitted from moving objects, the location, direction, energy, and time are stored at the time of fission or activation and then at the time of emission, the geometry configuration is updated to provide the correct location and orientation of the delayed particle.

2.6.2 MCR2S with Geometry Movement

The Mesh Coupled implementation of R2S (MCR2S), developed by the Culham Science Center, was updated to allow geometry components to change location after shutdown [18]. This capability was developed to facilitate SDR calculation during maintenance and intervention activities. MCR2S relies on MCNP for both neutron and photon transport steps and FISPACT for the activation calculations. It allows multiple components to be moved to different locations prior to the photon transport step.

These geometry translations occur by creating a copy of the components that will move. Transform cards are applied to the copies. The original components remain in their original locations and their material is changed to vacuum. Any photon

source particle that starts in one of the components that moves after shutdown is automatically translated to the correct location.

The requirement that both the original component (set as void) and its transformed copy are present during the photon transport step means that there can be no overlap between the parts which could be problematic for small transformations.

2.7 Summary

The MC method is the most accurate way to obtain detailed distributions of the neutron and photon fluxes in FES, but it is necessary to use VR methods in order to efficiently calculate these results. This section has reviewed some of the most recent work in the fields of VR for SDR analysis and MC analysis of moving systems. GT-CADIS, the implementation of MS-CADIS specifically for SDR analysis, has been proven to effectively optimize the neutron transport step of R2S. Developments in MCNP6 and MCR2S that provide some capability for updating the position of geometry have also been discussed.

In the case of geometry movement after shutdown, the importance of the photons to the detector SDR changes over time. This requires an extension to GT-CADIS that takes the movement into account. This work aims to advance and combine the current work in these fields through the derivation of a time-integrated adjoint neutron source term that will ultimately optimize the neutron transport step in systems that undergo movement after shutdown.

Chapter 3

Time-dependent R2S

In certain applications, quantifying the shutdown dose rate is not only important when the device is in a static configuration, but also during operations that involve movement after shutdown. To produce time-dependent SDR results, the first two steps of the R2S workflow remain unchanged. The difference is in the photon transport step because the configuration of the geometry is changing after shutdown. This chapter will first discuss the tool developed to transform CAD geometries for radiation transport calculations. Then, the time-dependent (T)R2S workflow will be introduced. Finally, a demonstration will be shown.

3.1 Implementation

3.1.1 CAD Geometry Transformations

There are various scenarios that involve the motion of geometry components during a radiation transport simulation. One example is the movement of activated components of a fusion energy device during a maintenance operation. In this work, DAGMC is used to facilitate radiation transport directly on CAD geometries [19].

The surfaces of the CAD geometry are discretized into a triangular mesh and stored within MOAB [20]. Particle tracking occurs on the faceted representation of the geometry.

A tool was developed to generate stepwise CAD geometry files that capture the movement of components over time based on user-supplied motion vectors. This tool has application to this thesis work but is also a general purpose tool for any calculation in which the geometry configuration changes.

First, the original configuration of the geometry is built using CAD software, such as Trelis [21]. Any component that will move is tagged (labeled with metadata) with a transformation number. The transformation numbers correspond to motion data that are given in a separate text file. The components are tagged with as many transformation vectors as needed to specify the full path of motion. The text file containing the transformation information is formatted such that each transformation number corresponds to a velocity vector, start time, and stop time. The total time of motion and desired number of time steps are also given.

The geometry transformation tool is built upon the Mesh-Oriented datABase (MOAB) [20] which has has the ability to store and manipulate mesh data. Upon loading the geometry and transformation text file, MOAB functions are used to read the transformation number and starting position of each moving component, then update the position accordingly. A new geometry file is generated for each time step.

This tool only handles rigid-body transformations; no geometric deformations or scaling. It also does not handle objects kinetics, so the user must be careful to not cause any overlap of components during the geometry movement. A requirement of transport geometries is that each volume be fully closed; therefore this tool can only be used to move components that do not share any surfaces with other non-moving

components to ensure that the transformation does not create any open volumes. The new geometry files that contain stepwise changes of the geometry configuration are used as input for transport calculations.

3.1.2 Workflow

This section outlines the workflow for generating time-dependent SDR maps. Essentially, a single neutron transport calculation is performed on the geometry in its original configuration and a photon transport calculation is performed in the original configuration and then at each of N discrete time steps of geometry movement. The main operations of the time-integrated (T)R2S method are listed below and a full implementation flowchart is given in Fig. 3.1.

1. MC neutron transport simulation on geometry at time step $t_{mov} = t_0$
2. Activation analysis
3. MC photon transport simulations on geometry at each time step $t_{mov} = t_0..t_N$

To perform the TR2S process, a transport geometry and a conformal tetrahedral mesh are first generated using CAD software and tagged with the same transformation numbers. Neutron transport is performed via DAG-MCNP and the mesh is used to score the energy-wise neutron flux.

The neutron flux tally along with an irradiation and decay scenario of interest are given as input to the PyNE R2S script to generate ALARA [12] input files. ALARA generates a photon source file for each decay time of interest. The conformal tetrahedral mesh tagged with transformation numbers along with the ALARA photon source files are converted to tetrahedral mesh based sources by the PyNE R2S script.

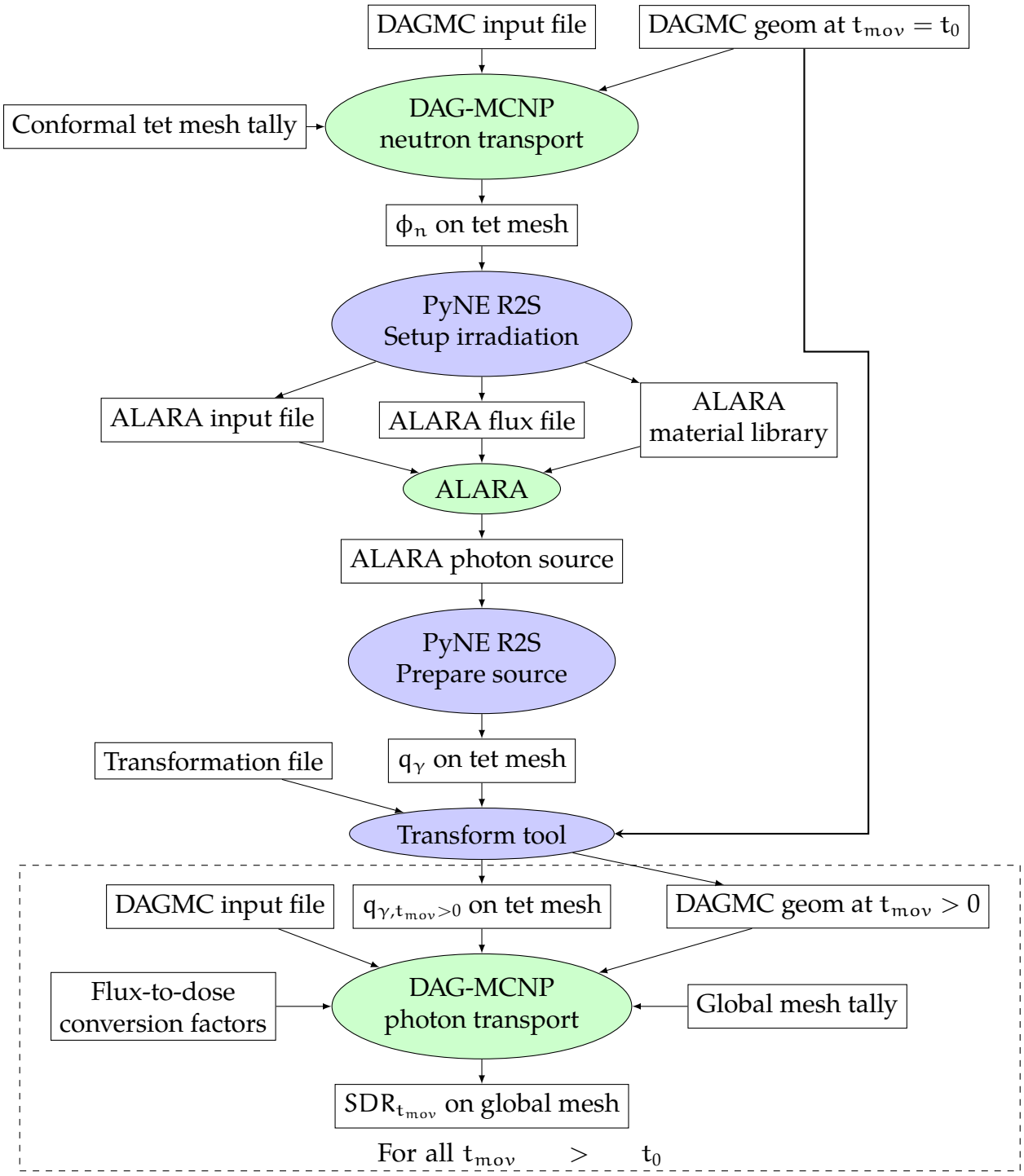

Figure 3.1: Time-integrated R2S (TR2S) workflow for calculating the SDR at each time step of geometry movement after shutdown, t_{mov}. Scripts are shown in blue ovals, physics codes in green ovals, and files in white rectangles.

Because all source mesh files generated reflect the original position of the geometry, they need to be transformed to the correct locations for each time step, t_{mov}, with the transformation tool. DAG-MCNP is compiled using the custom mesh-based source sampling routine and the transformed sources and geometries are then used as input for the MC photon transport simulations. A global photon flux mesh tally, modified with flux-to-dose rate conversion factors, is used to score the SDR at each time step.

3.2 TR2S Demonstration

To test the implementation of the mesh-based TR2S workflow, a simple demonstration problem was developed and the time-dependent SDR was calculated.

3.2.1 Problem Description

The source, geometry, and materials used in this experiment were chosen to have similar features to those found in fusion energy devices. A planar view of the geometry is shown in Fig. 4.1. It is composed of a chamber with a central cavity measuring 2 m x 2 m x 2 m. The walls are 2 m thick. A modular block measuring 1.46 m x 1.46 m x 1.46 m is cut out from one side of the chamber. There is a 2 cm gap between the modular block and the chamber to avoid any shared surfaces between moving and static components. The chamber and modular block are composed of a mixture of 20 vol % Stainless Steel 316 (SS-316) and 80 vol % helium. While not a realistic material, enough activation occurs in the SS-316 to produce interesting results while the mix with helium facilitates faster radiation transport simulations, desirable for this demonstration. The chamber is surrounded by vacuum and there is helium in the central cavity.

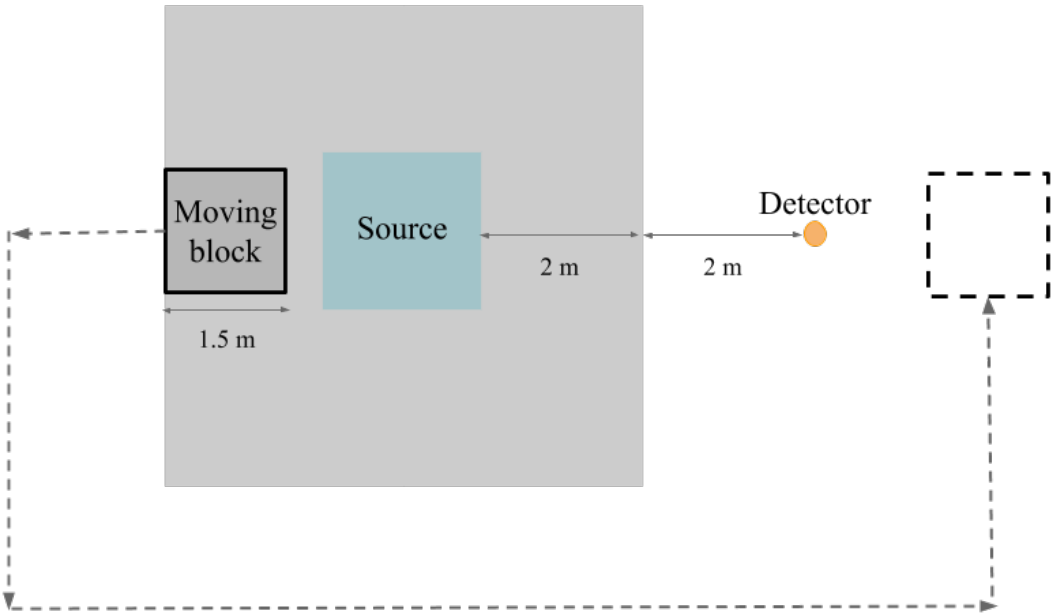

Figure 3.2: Planar view of the geometry. Stainless steel and helium chamber with 2 m thick walls, modular component cut-out, and central cavity measuring 2 m x 2 m x 2 m. The central cavity is filled with helium and the chamber is surrounded by vacuum. A SDR detector is located 2 m in the x-direction from the chamber. The path of geometry movement is shown by the dashed line.

An isotropic neutron source filled the central cavity. It was sampled uniformly in space and within the energy interval of 13.8-14.2 MeV. The source intensity was chosen to be 10^{16} neutrons/s. The SDR was measured with a detector after a single pulse irradiation of 365 days and decay period of 30 days. The detector is a sphere, 10 cm in radius, located 2 m in the positive x-direction away from the outer wall of the chamber. The detector is composed of 52.34 at. % H-1, 47.66 at. % C-12.

A CAD model and tetrahedral mesh model of this geometry were built using Trelis. All components were tagged with material names and the modular component was also tagged with four transition numbers each representing a segment of the path of movement. The faceted geometry file was exported via the DAGMC Trelis plugin [19], [21]. The block moves at a speed of 100 cm/s and takes 27 s to

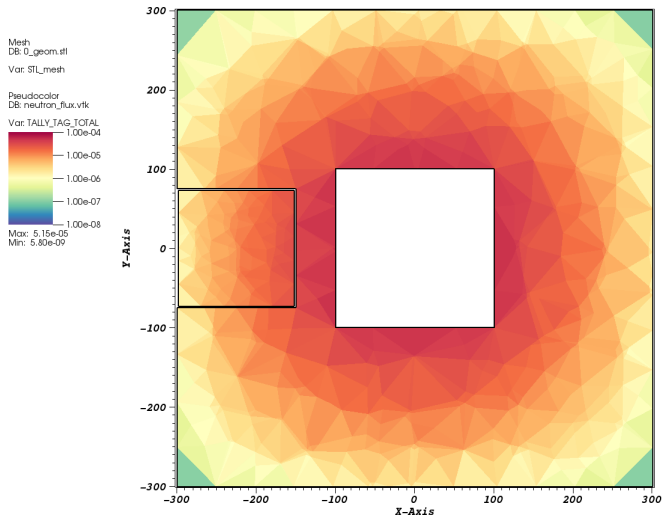

Figure 3.3: Total neutron flux $[n/(cm^2 \cdot s)]$ in the original configuration of the geometry.

move from the original to final location. Because the movement happens 30 days after shutdown and occurs over a relatively short time period, source decay is not taken into account in this experiment.

The changing dose rate at the detector was calculated as well as global maps of the dose accumulating over time. The path was divided into 32 time steps and a photon transport calculation was performed at each step. To determine the effect of the level of discretization of the movement, the accumulated dose from the 32-step simulation will be compared to 16- and 8-step versions of the movement.

3.2.2 Time-dependent SDR Maps

A 175 group VITAMIN-J energy structure [22] was applied to a conformal tetrahedral mesh tally in order to achieve both a spatial and energy-wise distribution of the neutron flux. The total flux is shown in Fig. 3.3. As expected, the flux is strongest at the inner wall of the steel chamber near the source and dissipates outwards from there.

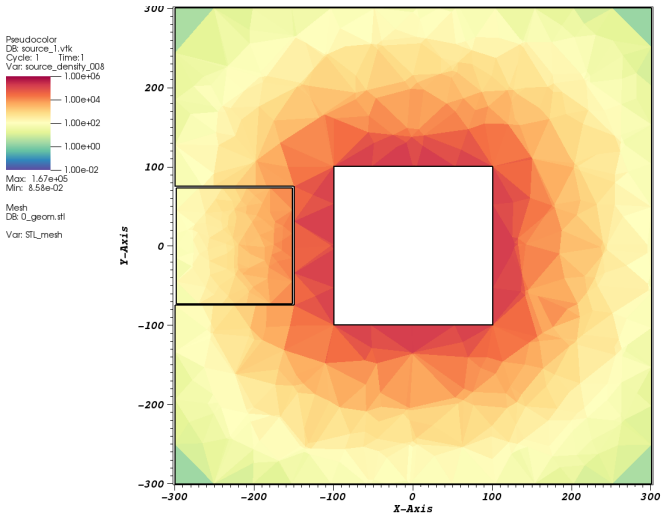

Figure 3.4: Photon source density $[\mathrm{p}/(\mathrm{cm}^3 \cdot \mathrm{s})]$ in the original configuration of the geometry.

The photon source resulting from the ALARA calculation using the neutron flux as input is shown in Fig. 3.4. Because neutron activation results in photon emission, the photon source is also strongest near the center of the chamber and the right side of the moving block.

The photon dose rate was scored at the detector location and the results from each time step are shown in the plot in Fig. 3.5. The dose rate is initially steady from steps 1 through 15, begins to increase to a peak value around step 20, then decreases. The initial steady period is caused by the photons from the static chamber; photons from the moving block are not causing an effect. The dose rate rises as the block moves closer to the detector and is not shielded by the static chamber. Because the source intensity is strongest on the right side of the block, the dose rate at the detector falls as the block moves upwards towards the detector, shielding it from the strongest source.

The photon dose rate was also scored on a global mesh at each time step. A dose accumulation script was used to calculate the dose over time. The results from the

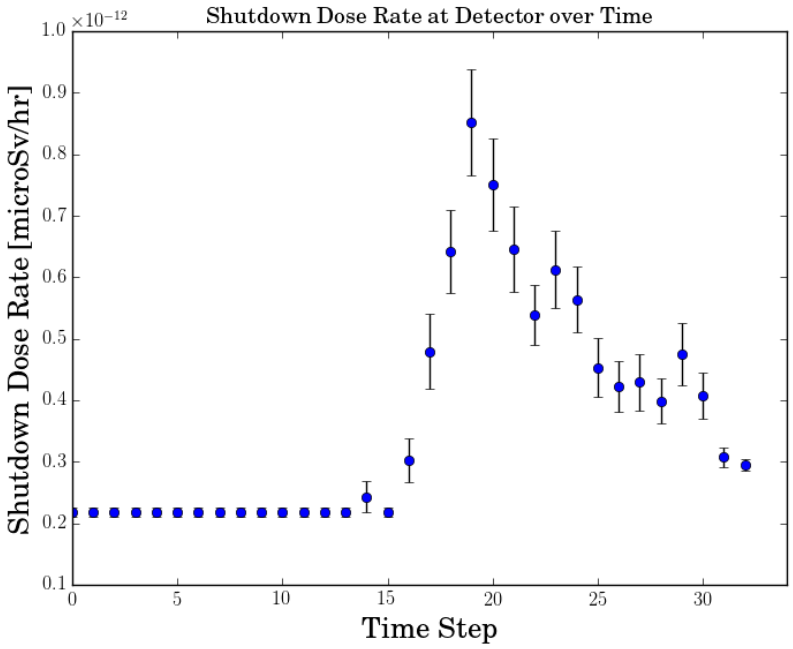

Figure 3.5: Photon dose rate [$\mu Sv/hr$] at detector location recorded at each time step.

16-step calculation are shown in Fig. 3.6. The final accumulated dose from the 32-, 16-, and 8-step calculations are shown in Fig. 3.7.

The percent difference in final accumulated photon dose between the 32-step and 16- and 8-step simulations is shown in Fig. 3.8. There are large differences along the path of movement, but very small near the detector. The minimal differences at the detector location caused by time-step discretization can also be seen in Fig. 3.9 which compares the accumulated dose over time across 32-, 16-, and 8-step simulations.

3.3 Summary

Performing the TR2S method can give insight into the dose rate along the proposed path of movement of activated components and the dose that accumulates in the

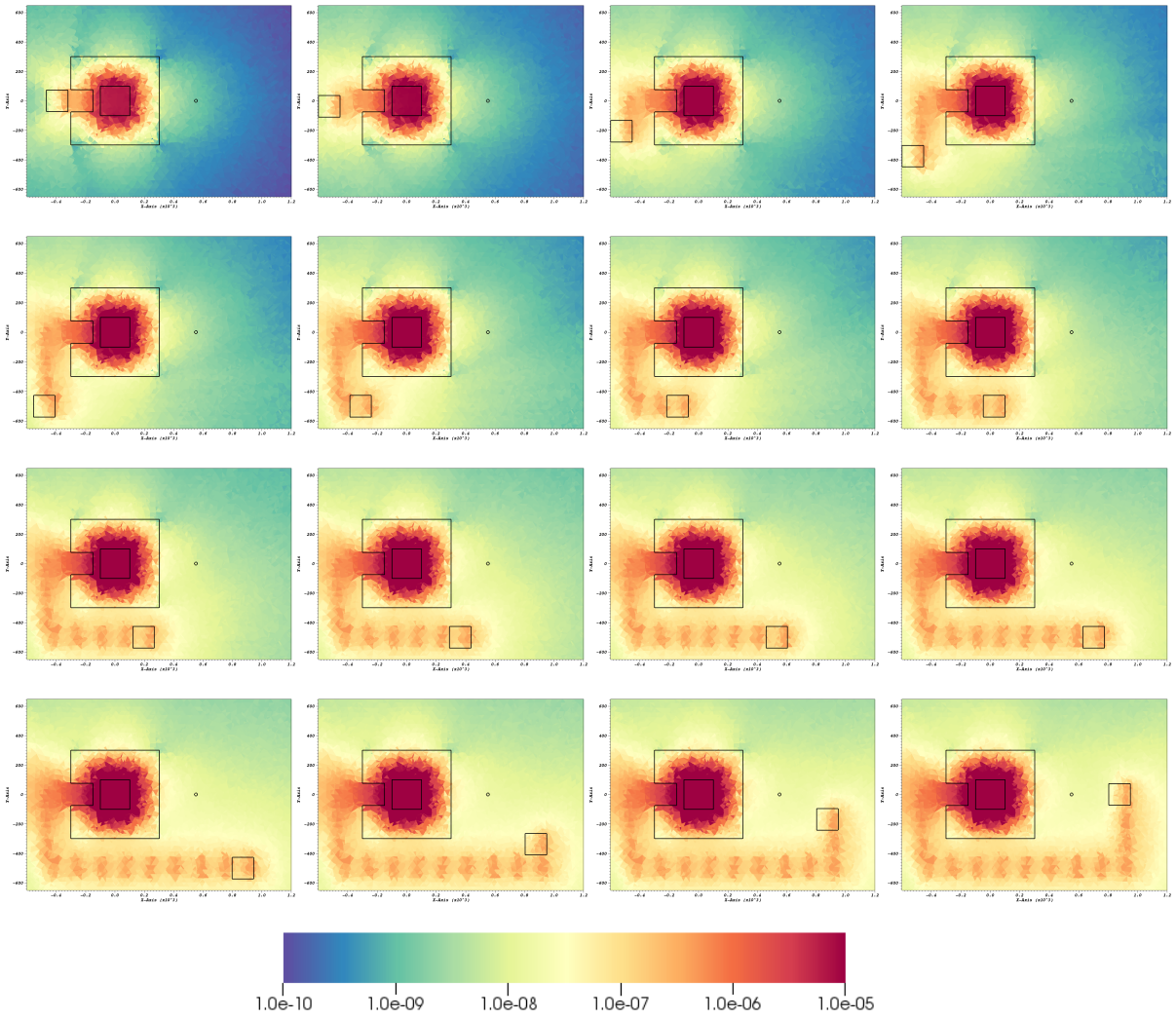

Figure 3.6: Accumulated photon dose resulting from 16-step simulation.

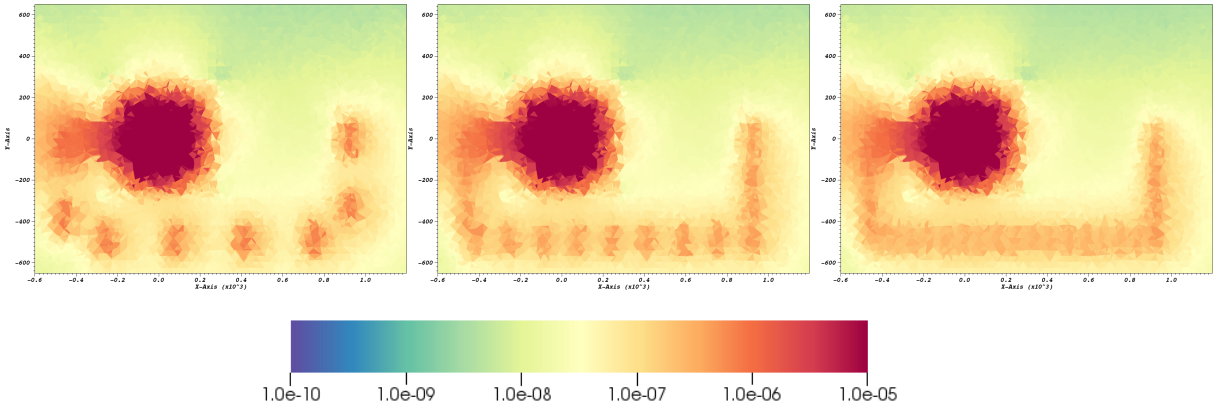

Figure 3.7: Left to right: Accumulated photon dose resulting from 8-, 16-, and 32-step simulations.

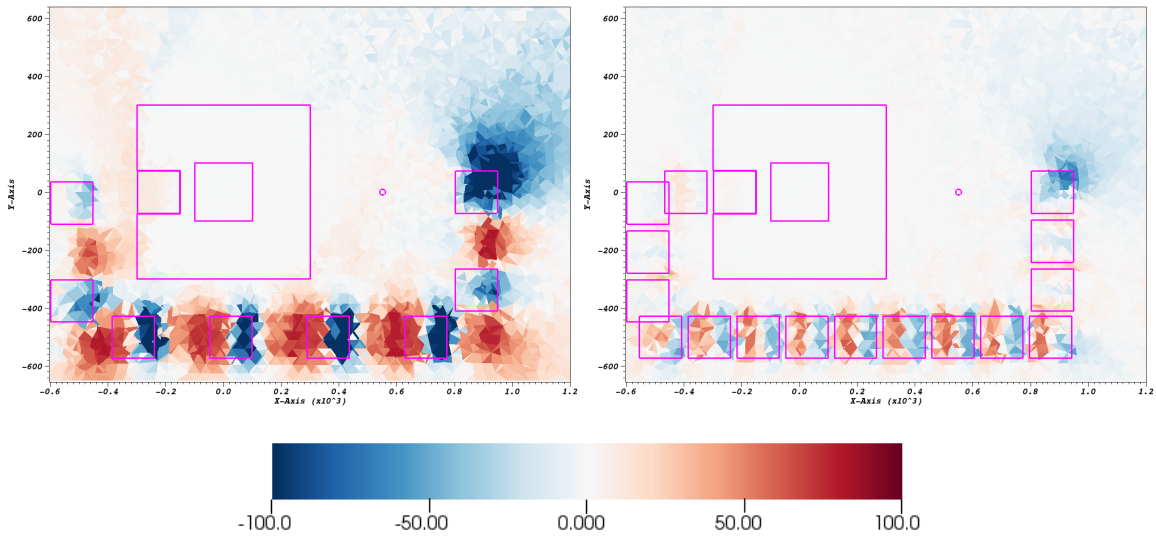

Figure 3.8: Percent difference of total accumulated dose between the 32-step and 8-step simulations (left) and the 32-step and 16-step simulations (right).

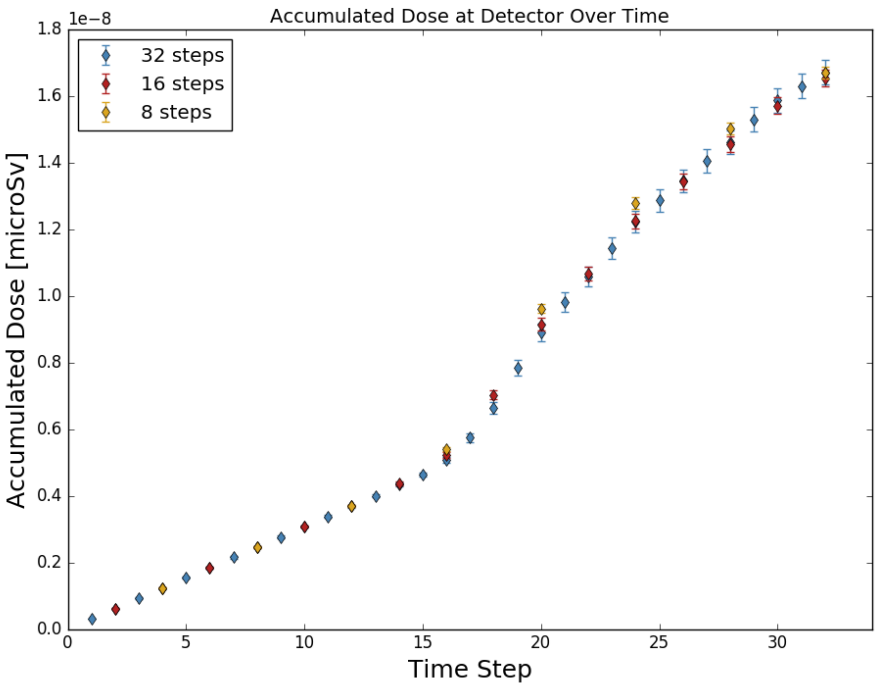

Figure 3.9: Accumulated dose at the detector location over time for the 32-, 16-, and 8-step simulations.

facility over time. This information can be beneficial in maintenance planning when determining the how soon after shutdown the component can move and the best path around the facility for limiting the dose to sensitive regions.

The number of time steps simulated will be decided by the user based on problem-specific variables. It is suggested that first the path is coarsely discretized and then based on the dose over time in the most sensitive regions, the user can choose to update the level of discretization or not. Ultimately, the time steps chosen need to capture the features of the path that will cause significant contributions to the dose at the detector location(s). This depends on several factors including the shape of the path, the source strength, the medium of transport, the speed of geometry movement, the distance between the activated component and the detector, and the

direction of travel relative to the detector.

Chapter 4

Demonstration of GT-CADIS

GT-CADIS has proven to be an effective method for optimizing the neutron transport step of SDR analysis in static FES when the SNILB criteria are met [3]. As it stands, this method will not provide appropriate VR parameters for the cases where activated components are moving after shutdown. The following experiment will demonstrate the need for a time-integrated adjoint photon solution in order to provide useful VR parameters for dynamic systems.

4.1 Problem Description

The model chosen for this demonstration is very similar to that used in the TR2S demonstration in Section 3.2. A planar view of the geometry is shown in Fig. 4.1. In this demonstration, the chamber material is solid Stainless Steel 316, there is no moving block, and the chamber is surrounded by air. The source and detector are the same. The SDR was measured after a single pulse irradiation of 10^5 s and decay period of 10^5 s.

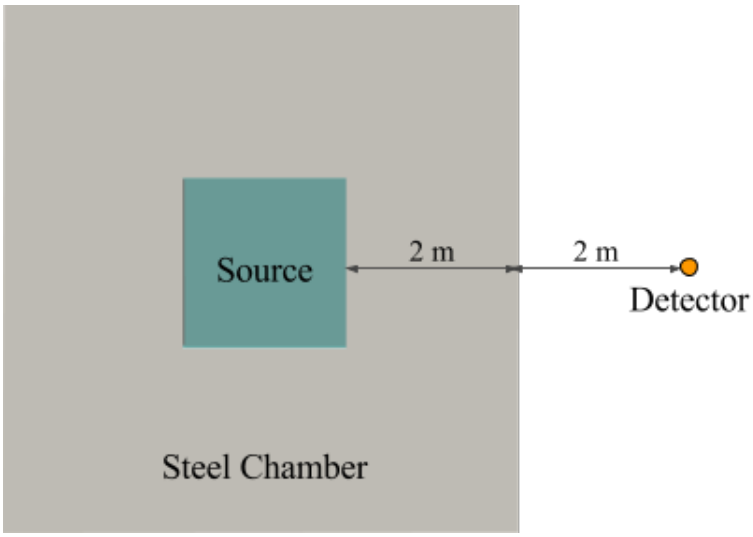

Figure 4.1: Planar view of the geometry. Steel chamber with 2 m thick walls and central cavity measuring 2 m x 2 m x 2 m. The central cavity is filled with helium and the chamber is surrounded by air. An SDR detector is located 2 m in the x-direction from the chamber.

First, the R2S workflow was performed with analog [1] MC neutron and photon transport steps. Then, the GT-CADIS method was used to generate VR parameters to optimize the neutron transport step.

4.2 Analog R2S

The main steps of the R2S workflow are as follows:

1. MC Neutron Transport
2. Activation Analysis
3. MC Photon Transport

MCNP5 [5] was chosen as the MC code and ALARA [12] as the activation code.

[1] In all demonstrations, analog transport includes implicit capture.

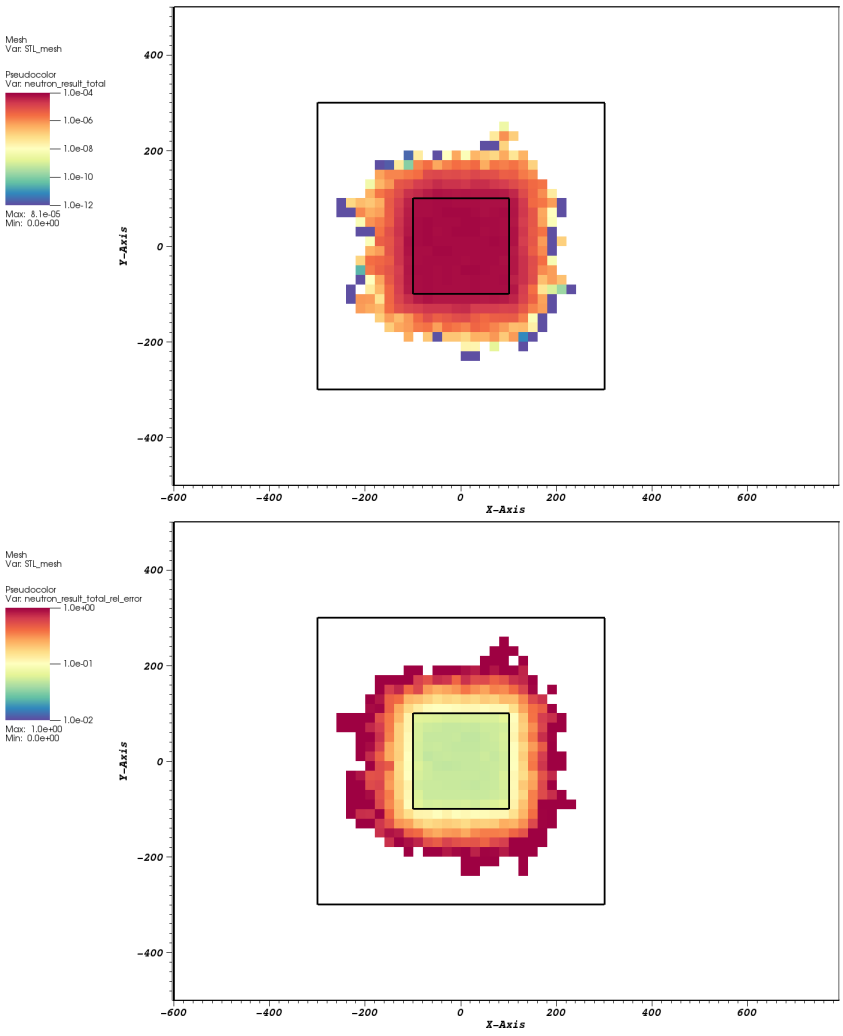

Figure 4.2: Neutron flux (top) and relative error (bottom) resulting from analog MC simulation.

First, a DAGMCNP5 [19] simulation with 10^7 histories was run using the CAD geometry generated by Trelis and an input file that contained a Cartesian mesh tally over the entire geometry to score neutron flux. Again, a 175 group energy structure was applied to the mesh tally in order to achieve both a spatial and energy-wise distribution of the neutron flux. The resulting total neutron flux and relative error are shown in Fig. 4.2.

A script in PyNE's R2S module was used to generate the ALARA input files

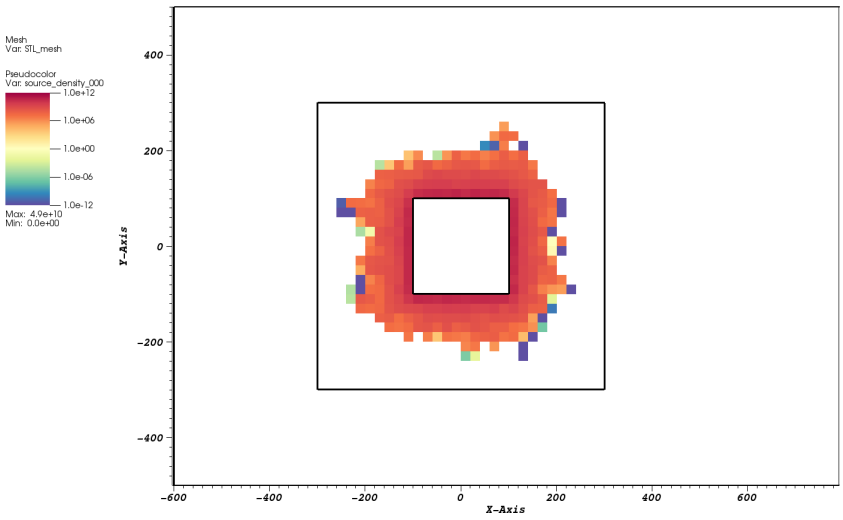

Figure 4.3: Photon source generated by ALARA activation calculation using the analog MC neutron transport result.

using the neutron flux mesh. ALARA was run using FENDL2.0 nuclear data [23]. PyNE R2S was used again to generate a mesh-based photon source from the ALARA output. The photon source is shown in Fig. 4.3.

4.3 GT-CADIS VR Parameters

To optimize the neutron transport step of R2S, the GT-CADIS method was used to generate a biased source and weight windows. The main steps of the GT-CADIS method are as follows:

1. Deterministic adjoint photon transport
2. Calculation of the GT-CADIS adjoint neutron source
3. Deterministic adjoint neutron transport
4. Generation of biased source and weight windows from adjoint neutron flux

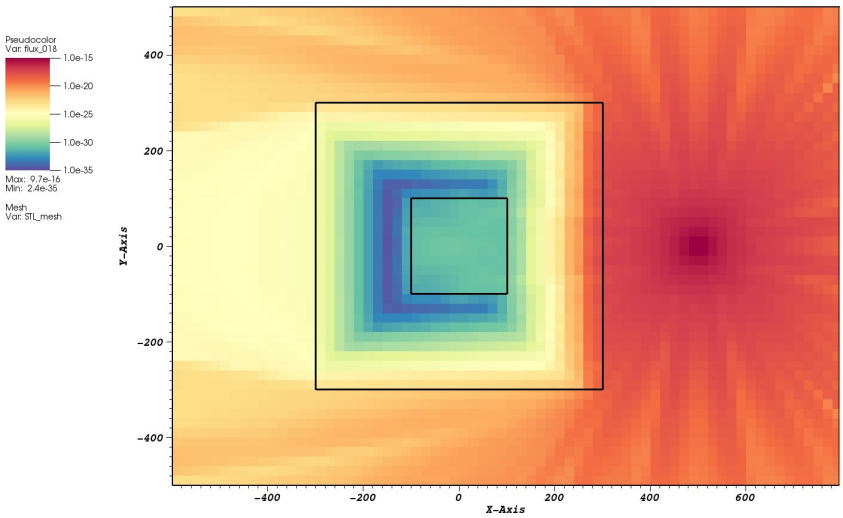

Figure 4.4: Adjoint photon flux used to generate adjoint neutron source according to the GT-CADIS method.

The S_N code PARTISN [24] was used to perform the adjoint transport steps. The source for adjoint photon transport was a 42 energy group VITAMIN-J discretization of the ICRP-74 flux-to-dose conversion factors [25]. The resulting adjoint photon flux mesh is shown in Fig. 4.4.

Next, the coupling term T was calculated for each material. This was done by performing separate ALARA simulations for each of 175 neutron energy groups in each of the materials to obtain the photon source in each photon energy group as a function of the neutron flux in each neutron energy group. T was then calculated using Eq. 2.28.

This T was combined with the adjoint photon flux to generate the GT-CADIS adjoint neutron source via Eq. 2.27. PARTISN was run again using this adjoint neutron source and the resulting adjoint neutron flux for the 13.8-14.2 MeV energy group is shown in Fig. 4.5.

This adjoint neutron flux functions as an importance map of neutrons to the final SDR. In the region of the chamber near the detector, there is a high adjoint flux,

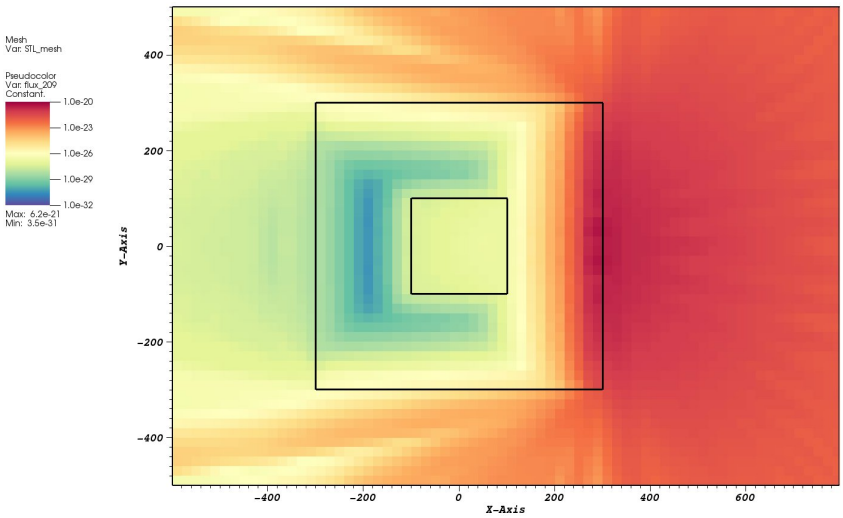

Figure 4.5: Adjoint neutron flux used to generate the biased source and weight windows according to the GT-CADIS method.

therefore neutrons in this region have a high importance to the SDR. In contrast, there is a low flux in the regions on the far side of the detector. Neutrons in this region are less likely to activate materials that will then produce decay photons that contribute to the SDR.

The adjoint neutron flux was then used to generate the biased source and weight windows via the CADIS method. These are seen in Fig. 4.6 and Fig. 4.7.

The biased source and weight windows were used to optimize the neutron transport step of R2S. A DAGMCNP5 simulation with 10^7 histories was performed using these VR parameters and the resulting neutron flux and relative error are shown in Fig. 4.8.

ALARA was run using the neutron flux and a 1y irradiation time and 30d decay scenario. The photon source distribution generated is shown in Fig. 4.9.

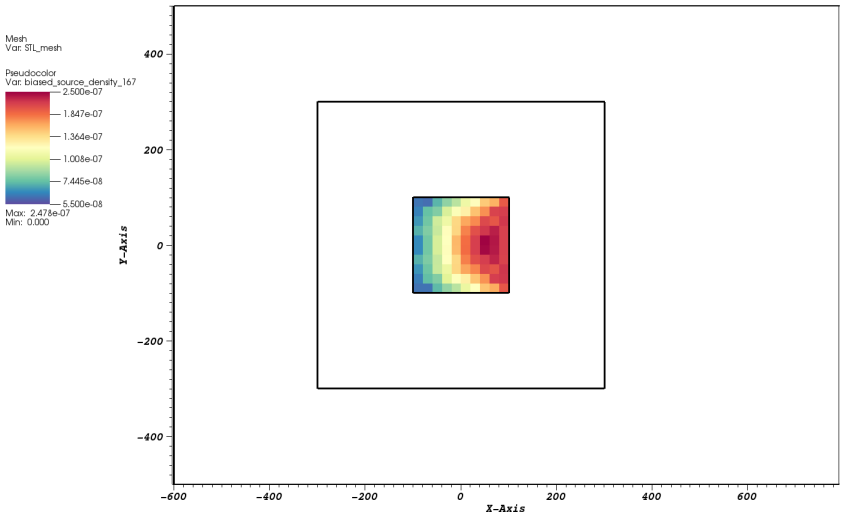

Figure 4.6: Biased neutron source generated with GT-CADIS method.

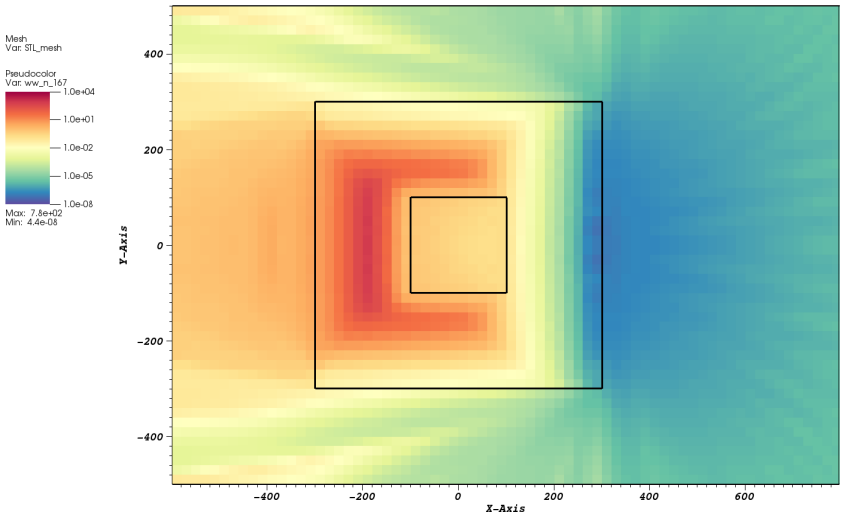

Figure 4.7: Weight window mesh generated with GT-CADIS method.

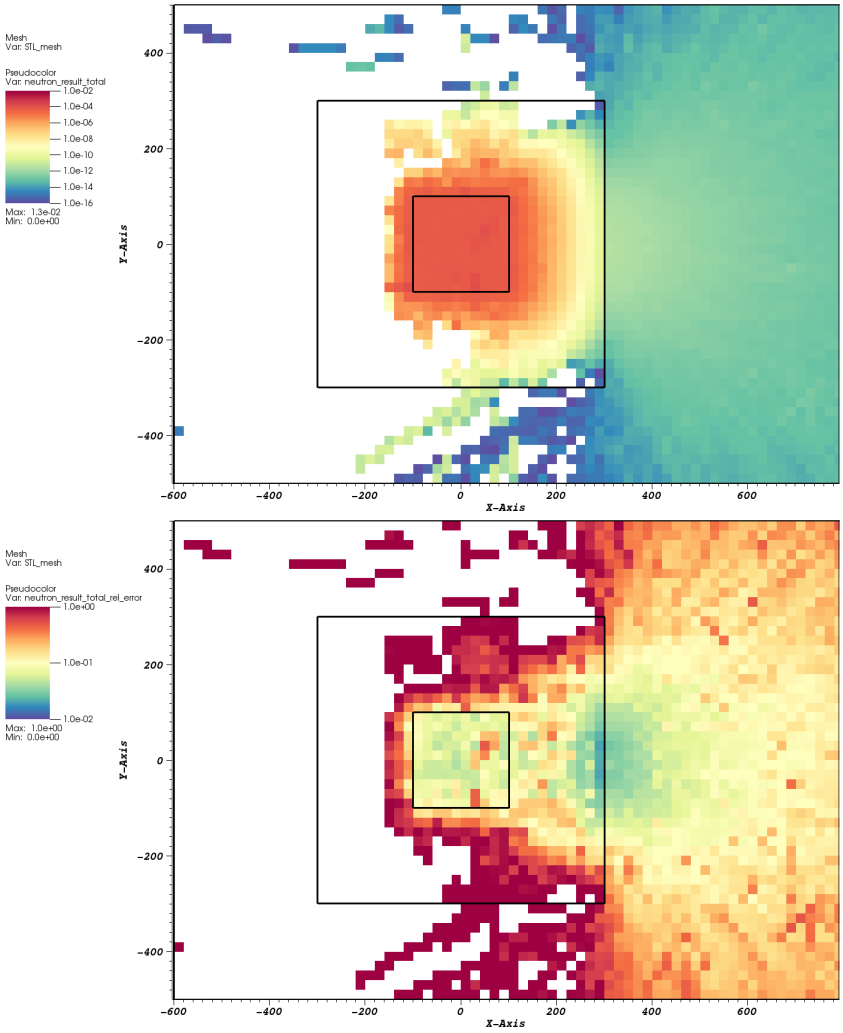

Figure 4.8: Neutron flux and relative error resulting from MC simulation using GT-CADIS biased source and weight window mesh.

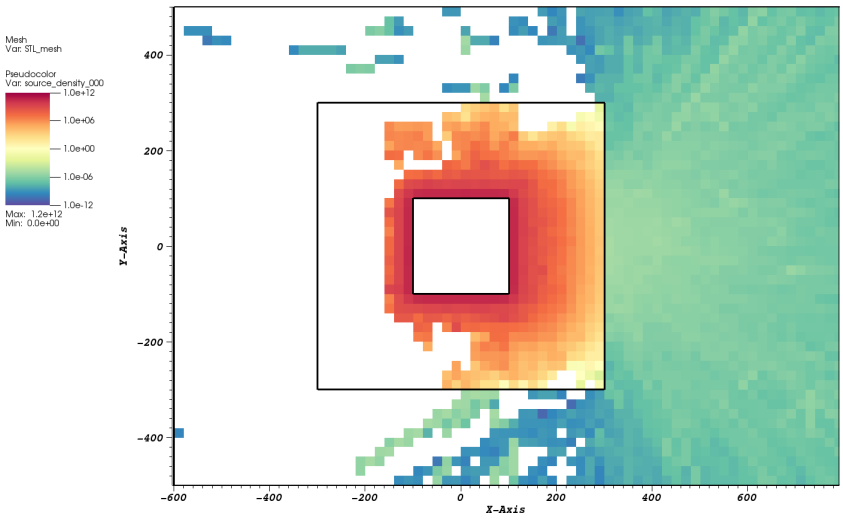

Figure 4.9: Photon source generated after ALARA activation calculation using the GT-CADIS optimized neutron transport result.

4.4 Limitations of GT-CADIS for Moving Systems

Comparing the neutron flux and relative error obtained by the analog MC transport in Fig. 4.2 and that obtained using the GT-CADIS method in Fig. 4.8, it is clear to see that given the same number of histories, the GT-CADIS method not only reduces the error in regions of the chamber that are important to the SDR, but allows a solution to be calculated in the detector region.

Now, consider if the steel chamber was not a monolithic block, and instead made of modular components that can move after shutdown, during the photon decay process. For example, a component of the chamber originally located on the far side of the detector moves to a location near the detector as shown in Fig. 4.10. The photons produced in the activated, moving component become more likely to contribute to the SDR as the component moves closer to the detector. This also means that the neutrons in this region are important because it is the neutron irradiation that results in photon emission.

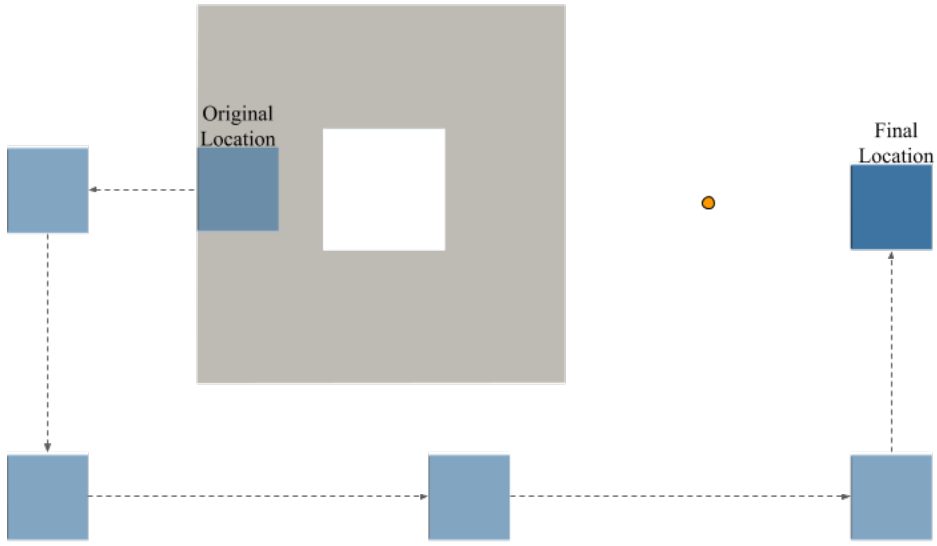

Figure 4.10: Path of activated component moving from the far side of the SDR detector to position next to it.

Highlighting the region of the moving component in the adjoint neutron flux map produced by GT-CADIS, Fig. 4.11, it can be seen that this is no longer a valid importance map of the neutrons to the final SDR. There is a low adjoint flux, therefore low importance in the moving component that will eventually be positioned near the detector. Because this adjoint neutron flux is used to generate source and transport biasing parameters, neutrons will be steered away from interactions in this component, increasing the uncertainty in a region that will ultimately be important to the SDR.

4.5 Summary

In this demonstration, it was shown that the GT-CADIS method is insufficient for scenarios that involve movement after shutdown, during photon transport. A successful extension to this method that takes the movement into account will give

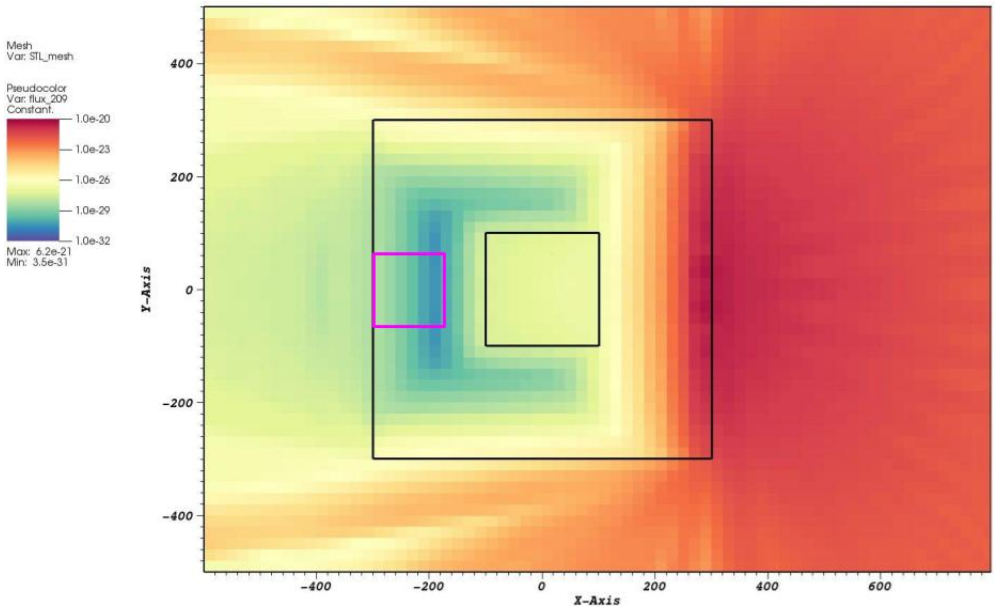

Figure 4.11: Adjoint neutron flux map with region of moving component highlighted.

appropriate importance to regions that will make significant contributions to the detector SDR.

Chapter 5

Variance Reduction for Time-integrated Multi-physics Analysis

The MS-CADIS method of variance reduction was developed to optimize the primary radiation transport in a coupled, multi-step process. The first implementation of this method was applied to the coupled neutron activation-photon decay process that occurs in FES. In its current form, MS-CADIS is only applicable to static systems where the geometry remains unchanged in all steps of the multi-step process.

This chapter will first discuss MS-CADIS outside of the context of SDR analysis. Next, a time-integrated solution to the adjoint of the physical process occurring during geometry movement will be derived. This time-integrated solution will then be applied to the GT-CADIS method to form the Time-integrated (T)GT-CADIS adjoint neutron source that will ultimately be used to optimize the neutron transport step of SDR analysis.

Finally, the implementation of the TGT-CADIS method will be discussed and it

will applied to a simple problem to demonstrate its efficacy.

5.1 Generalized MS-CADIS Method

In the current literature, MS-CADIS is primarily discussed as it applies to SDR analysis [2]. In actuality, MS-CADIS has always been intended to apply to any multi-step process in which the primary radiation transport is coupled to any secondary physical process. The addition of time integration to this methodology can also be applied to any coupled, multi-physics process. For this reason, it is prudent to discuss MS-CADIS in a more generalized manner.

The operator notation of the Boltzmann transport equation:

$$H\phi(u) = q(u) \tag{5.1}$$

where H operates on the particle flux ϕ and q is a source of particles, will be used to describe the primary radiation transport defined over a phase space u.

An equation of the same form, Eq. 5.2, where L operates on some function Ψ and b is a source term, will be used to describe a generic secondary physics, defined on a potentially different phase space, v:

$$L\Psi(v) = b(v). \tag{5.2}$$

Because this is a coupled system, the source of secondary physics is a function of the primary particle flux, $b(v) = f(\phi(u))$.

The adjoint identity for the neutral particle transport equation given in Eq. 2.6 is valid for an arbitrary adjoint source function [4], therefore the secondary physics has an adjoint identity of the same form:

$$\langle \Psi^+, L\Psi \rangle = \langle \Psi, L^+\Psi^+ \rangle$$

$$\langle \Psi^+, b \rangle = \langle \Psi, b^+ \rangle \tag{5.3}$$

where $\langle \cdot \rangle$ signifies the integration over all phase space.

In order to complete the generalized MS-CADIS derivation, it is necessary to assume that all responses of interest for both the primary physics and the secondary physics can be expressed as inner products of their solutions with some specific response functions. Considering primary physics response M and secondary physics response N, there should be response functions, σ_M and ω_N, respectively, such that:

$$M(\phi) = \langle \sigma_M, \phi \rangle$$

$$N(\psi) = \langle \omega_N, \psi \rangle. \tag{5.4}$$

This is not strictly true in all cases. However, since the MS-CADIS method is used only to derive variance reduction parameters, it is only necessary that an approximation exist that is sufficiently accurate to provide benefit from such parameters. This benefit would need to be demonstrated in any specific application of MS-CADIS.

In particular, MS-CADIS requires this to be true of the relationship between the source term for the secondary physics and the solution to the primary physics:

$$b(v) = \langle \sigma_b(u, v), \phi(u) \rangle, \tag{5.5}$$

and of the relationship between the ultimate response of interest and the solution to the secondary physics:

$$R_{final} = \langle \omega_R(v), \psi(v) \rangle. \tag{5.6}$$

For either physics, when the adjoint source is defined to be equal to a particular response function, the adjoint solution can be interpreted as the importance function

for that particular response. Therefore, defining the adjoint source, b^+, as the response function, ω_R, and applying the adjoint identity to Eq. 5.6 results in:

$$R_{final} = \langle \omega_R, \psi \rangle = \langle b, \psi_R^+ \rangle, \tag{5.7}$$

where the subscript R denotes that the adjoint solution, ψ_R^+, is an importance function for response R.

Substituting Eq. 5.5 then gives:

$$R_{final} = \left\langle \, \langle \sigma_b(u, v), \phi(u) \rangle, \; \psi_R^+(v) \, \right\rangle. \tag{5.8}$$

By changing the order of integration between the phase space of the primary physics and that of the secondary physics, this can be rewritten as:

$$R_{final} = \left\langle \, \langle \sigma_b(u, v), \psi_R^+(v) \rangle, \; \phi(u) \, \right\rangle. \tag{5.9}$$

Once again invoking the adjoint identity gives:

$$R_{final} = \left\langle \, \langle \sigma_b(u, v), \psi_R^+(v) \rangle, \; \phi(u) \, \right\rangle = \langle q(u), \phi_R^+(u) \rangle, \tag{5.10}$$

if:

$$q^+(u) \equiv \langle \sigma_b(u, v), \psi_R^+(v) \rangle. \tag{5.11}$$

This implies that ϕ_R^+ describes the importance function of the primary physics to the response of the secondary physics, and can be used in the CADIS methodology to find VR parameters for the primary physics that will ultimately accelerate the statistical convergence of the secondary physics.

Consider the process of neutron-induced prompt photon production. In this case,

the function $\sigma_b(u, v)$ is the neutron-gamma production cross section, $\sigma_{n,\gamma}(E_n, E_\gamma)$. Because the transport equations for neutrons and photons are identical, this is generally implemented as a single-physics problem, in which the coupling term $\sigma_{n,\gamma}$ appears as a scattering-like term between neutrons and photons.

The primary focus of SDR analysis is the process of neutron-induced delayed gamma production. GT-CADIS provides a method for calculating $\sigma_b(u, v)$ when certain conditions (known as SNILB) hold true. In this case, $\sigma_b(u, v)$ is the coupling term $T(E_n, E_\gamma)$, an approximation of the transmutation process [3].

An additional implication of this derivation is that there exists a response function that allows the direct calculation/approximation of the secondary physics response from the primary physics solution, as expressed in equation 5.9. This is exact for prompt photons generated by a neutron source. For delayed photons, this provides the underpinnings of the D1S methodology and the more recent NASCA implementation [30].

5.2 Time-integrated MS-CADIS

If the configuration of the geometry is changing over time during the secondary physics, it will affect the construction of the adjoint radiation transport source, q^+.

The solutions to both forward and adjoint transport will be calculated in discrete volume elements, v. There is a solution to the adjoint secondary physics at each position and each time.

- $\vec{r}_v(t)$ Position of volume element v at time t
- $\Psi^+(\vec{r}_v(t), t)$ Adjoint flux in volume element v at time t

To solve for the adjoint radiation source in each volume element, q_v^+, the time-dependent solutions of the adjoint secondary physics are combined by integrating over time:

$$q_v^+ = \frac{\int_t \Psi^+(\vec{r}_v(t), t)\sigma_b(\vec{r}_v(t), t))\, dt}{\int_t dt}. \tag{5.12}$$

This time-integrated source term is then used for adjoint radiation transport to obtain ϕ_v^+.

5.3 Time-integrated GT-CADIS

GT-CADIS is an implementation of MS-CADIS that is specific to SDR analysis. It provides a method to calculate a coupling term, T, that relates the neutron flux to the photon source. T is then used to solve for the adjoint neutron source as shown in Eq. 2.27.

If the geometry configuration changes after shutdown, the time-integrated MS-CADIS methodology shown in the previous section can be applied to the GT-CADIS adjoint neutron source as shown in Eq.5.13:

$$q_{n,v}^+(E_n) = \frac{\int_t \int_{E_\gamma} T_v(E_n, E_\gamma, t)\phi_\gamma^+(\vec{r}_v(t), E_\gamma, t)\, dE_\gamma\, dt}{\int_t dt} \tag{5.13}$$

Adjoint photon transport at each time step during geometry movement, t, will provide the adjoint flux of photons of energy E_γ, in volume element v, at time t, $\phi_\gamma^+(\vec{r}_v(t), E_\gamma, t)$. $T_v(E_n, E_\gamma, t)$ is the T value of the material in volume element v, at time t.

A T value is calculated for each decay time of interest, but for many practical problems, T will not change over the course of geometry movement because the time constants of decay and geometry motion are very different. The motion of

components occurs over a very short period of time relative to photon decay. This is assuming that the geometry movement will not begin until at least 10^5s, about one day, after shutdown when the remaining photons have longer half-lives. If the geometry movement spans long enough that source decay needs to be taken into account, the total time of movement is discretized into as many decay times as needed to resolve the difference. The geometry movement may be discretized more finely within the decay time period.

Using the discrete form of T in Eq. 2.28, the integral in Eq. 5.13 can be estimated by the sum:

$$q^{+}_{n,g,v} = \frac{\sum_{dt} \left(\sum_{h} T_{v,g,h,dt} \sum_{t_{mov}} \left(\phi^{+}_{\gamma,v,h,dt,t_{mov}} \right) \Delta t_{mov} \right)}{t_{tot}} \tag{5.14}$$

where t_{mov} is a time step after shutdown that corresponds to a change in geometry configuration, Δt_{mov} is the duration of the time step, and $\phi^{+}_{\gamma,v,h,dt,t_{mov}}$ is the adjoint flux of photons in energy group h, in volume element v, at that time step, and t_{tot} is the total duration of all the time steps.

5.4 Implementation

This section discusses the implementation of the time-integrated (T)GT-CADIS adjoint neutron source derived in the previous section.

5.4.1 TGT-CADIS Workflow

The first step of the TGT-CADIS workflow is the generation of a transport geometry and a conformal tetrahedral mesh using CAD software. Both geometries are tagged with transformation numbers that correspond to motion data and the transformation

tool is used to generate separate geometry files for each desired time step.

The geometry file at each time step, the adjoint photon source (the flux-to-dose rate conversion factors in the the detector location), and a Cartesian mesh that covers the entire geometry, are given as input into the PyNE GT-CADIS script to generate a PARTISN input file. Deterministic adjoint photon transport is performed resulting in a PARTISN output file of the adjoint photon flux in each photon energy group, h.

Because we ultimately need to combine the contribution from each time step in each volume element, the adjoint photon flux voxel mesh is mapped onto the conformal tetrahedral mesh of the geometry at that same time step using the mesh mapping tool described in Appendix A.2. Each tetrahedral mesh element has an ID associated with it. The ID numbers are consistent across the tetrahedral mesh files at each time step. This allows the contribution of the adjoint photon flux from each time step to be averaged in each tetrahedral mesh element:

$$\phi^{+}_{\gamma,v,h} = \frac{\sum_{t_{mov}} \phi^{+}_{\gamma,v,h,t_{mov}} \Delta t_{mov}}{t_{tot}}. \tag{5.15}$$

The time-integrated adjoint photon flux tetrahedral mesh is then mapped back on to a voxel mesh to use as input for the PyNE GT-CADIS script.

The PyNE GT-CADIS script is used to calculate a T value for each voxel, $T_{dt,v,g,h}$, using Eq. 2.28. To obtain the source of photons in each photon energy group, h, single pulse irradiations are performed with ALARA. Each material in the problem is irradiated with a single energy group of neutrons, g, and allowed to decay to the time of interest. The value of $T_{dt,v,g,h}$ is assigned to each voxel by finding the underlying material. If the voxel is composed of more than one material, the T value assigned is a volume-weighted average of the composite material. The process of calculating T is independent of the previously described steps, therefore can be

performed simultaneously.

Combining the calculated T with the time-integrated adjoint photon solution, yields the TGT-CADIS adjoint neutron source given by Eq. 5.14. The full implementation workflow is shown in Fig. 5.1. In the case that the geometry movement occurs during several decay periods, and therefore the time steps of movement are discretized to fit within these periods, the workflow will be performed for each decay time needed.

Once the TGT-CADIS adjoint neutron source has been calculated, deterministic adjoint transport is performed and an adjoint neutron flux PARTISN file is returned. The adjoint neutron flux functions as an importance map for the forward neutron transport. This map reflects the movement of geometry during the decay period and gives appropriate importance to regions that contribute to the SDR at any point during geometry movement. This adjoint neutron flux mesh is used to generate a biased neutron source and a weight window mesh via the CADIS method.

5.4.2 Fully-optimized, Time-integrated R2S Workflow

After the biased source and weight window mesh are generated with the TGT-CADIS method, they are used to optimize the forward neutron transport step of TR2S.

The next steps of the TR2S process, from activation analysis through photon source generation, are performed. At this point, there is a mesh-based photon source that corresponds to the geometry configuration at each time step of movement.

The source mesh file along with the previously generated adjoint photon flux mesh at each time step are used to generate a biased photon source and weight window mesh via the CADIS method. These VR parameters along with the DAGMCNP

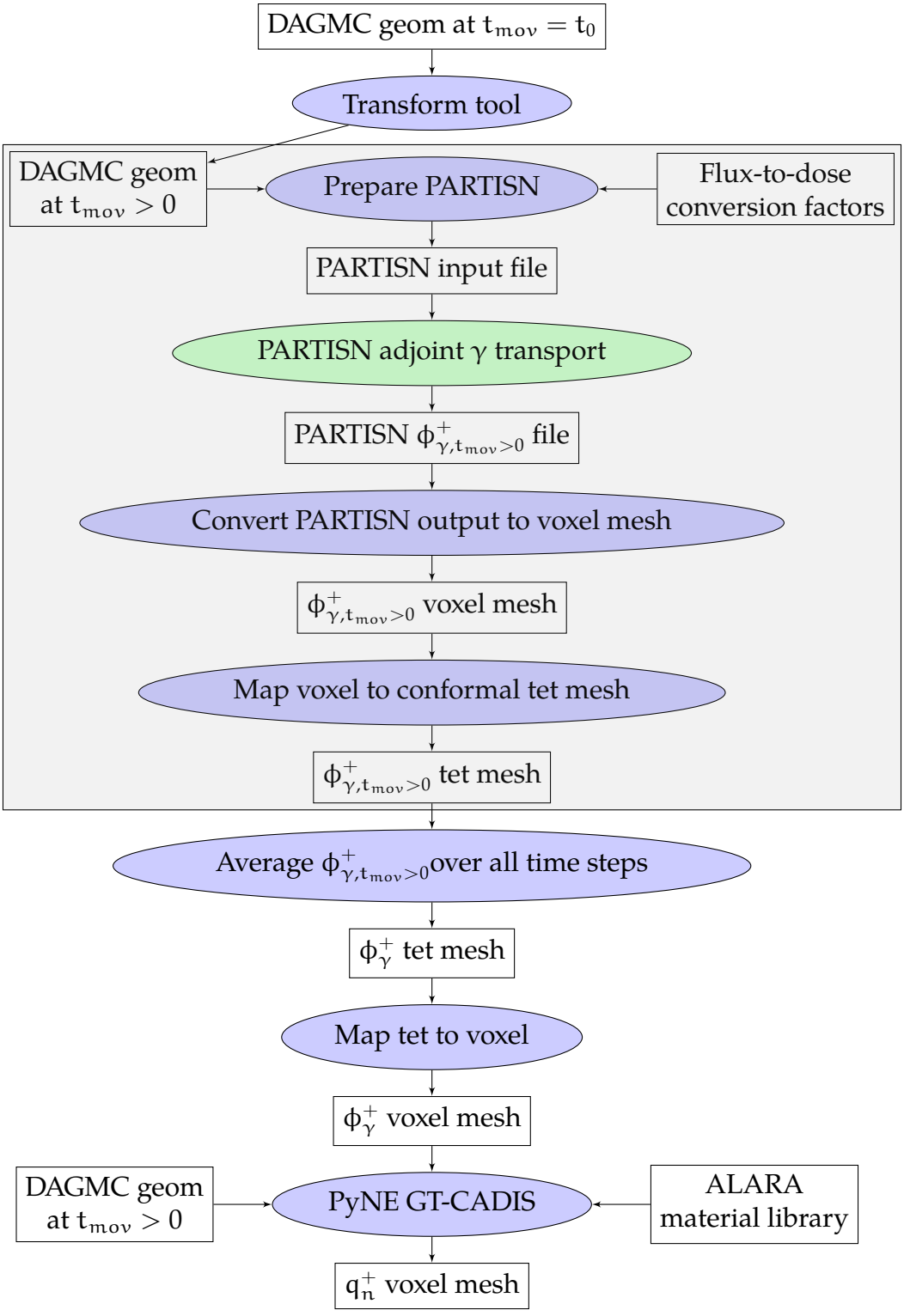

Figure 5.1: Workflow for generating the optimal adjoint neutron source via the time-integrated (T)GT-CADIS method. Scripts are shown in blue ovals, physics codes in green ovals, and files in white rectangles. Section in gray box performed for each time step of movement.

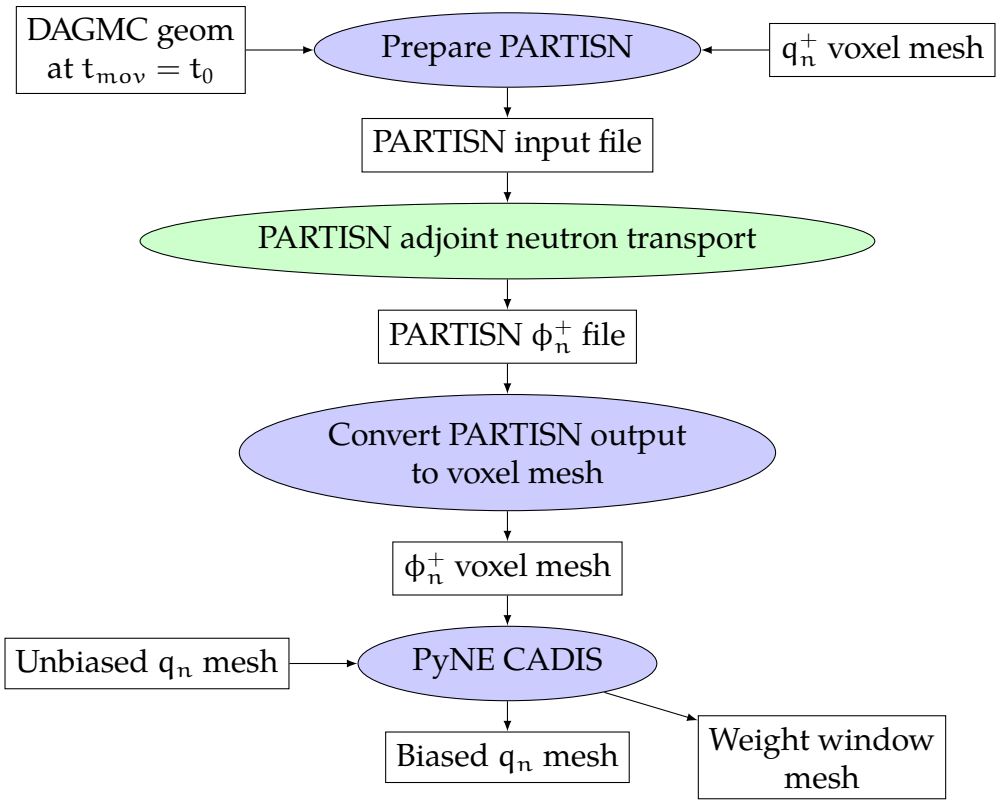

Figure 5.2: Workflow for generating a biased source and weight windows to optimize the neutron transport step of TR2S. Scripts are shown in blue ovals, physics codes in green ovals, and files in white rectangles.

input file are used as input for DAGMCNP photon transport. This results in a SDR map at each time step, t_{mov}.

The TGT-CADIS biased source and weight windows can be used to optimize the neutron transport and the CADIS method can be used to optimize each photon transport step. The fully optimized TR2S implementation is shown in Fig. 5.3.

5.5 Comparing TGT-CADIS, FW-CADIS, Analog

To demonstrate the efficiency of the TGT-CADIS method in optimizing the neutron transport step of TR2S, a simple problem was used to compare it against an analog

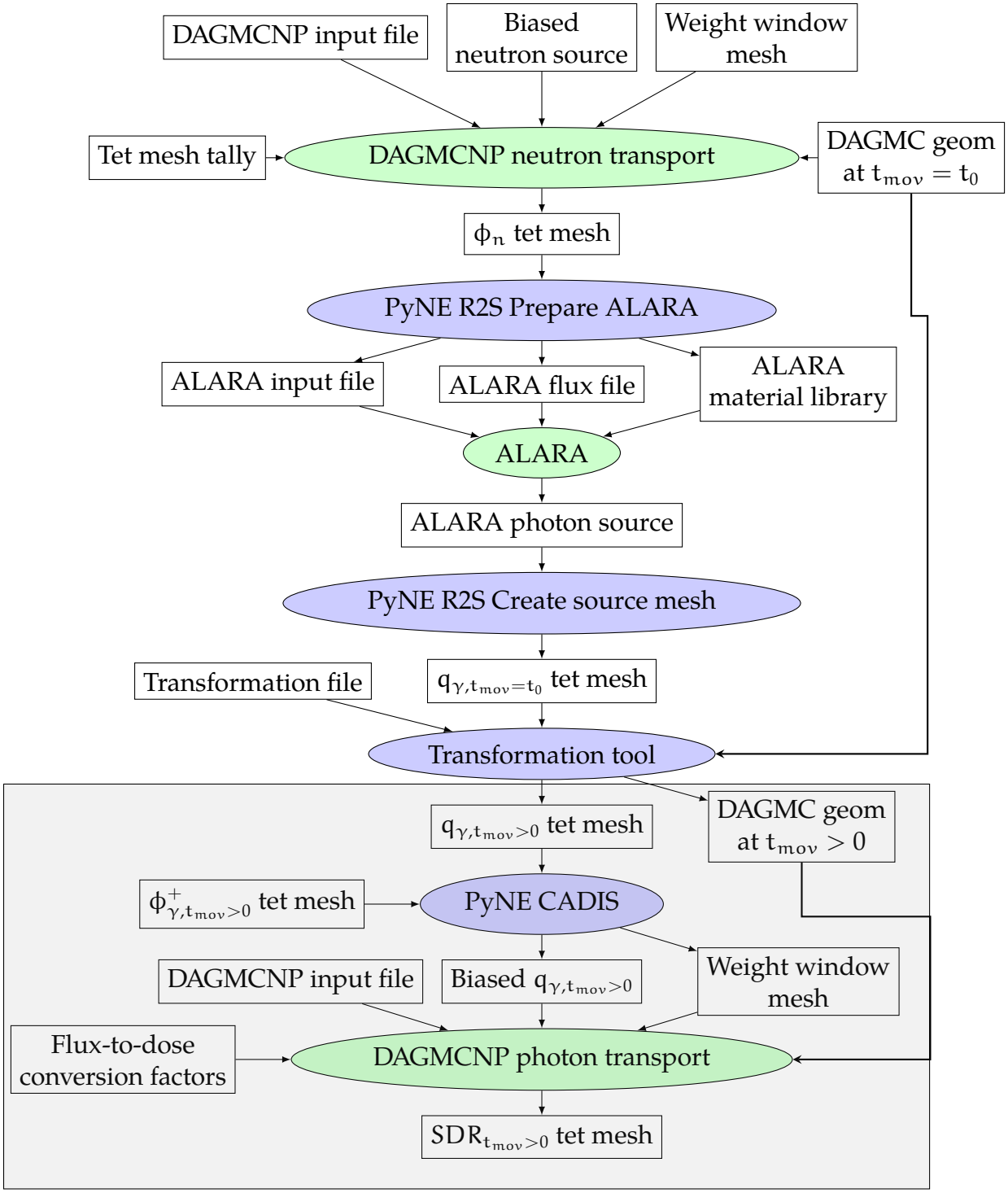

Figure 5.3: Fully optimized, time-integrated (T)R2S workflow for calculating the SDR. This workflow uses the TGT-CADIS biased source and weight windows to optimize the neutron transport and the CADIS method to optimize the photon transport steps. Scripts are shown in blue ovals, physics codes in green ovals, and files in white rectangles. Section in gray box performed for each time step.

simulation and one using FW-CADIS VR parameters. The error in the neutron flux and FOM were compared.

5.5.1 Problem Description

A planar view of the geometry is shown in Fig. 5.4. The geometry used in this experiment is a chamber with 2m thick walls and a central cavity measuring 2m x 2m x 2m filled with helium. The chamber is split in half with the right side (closer to the detector) composed of a mixture of a 15% Stainless Steel 316 (SS-316) and 85% helium by volume. The left side is composed of mixture of 75% SS-316 and 25% helium by volume. The left side also contains a modular block measuring 1.46 m x 1.46 m x 1.46 m that moves after shutdown according to the path in Fig.5.4. There is a 2 cm gap between the modular block and the chamber to avoid any shared surfaces between moving and static components. A 1.5m thick SS-316 wall was placed between the chamber and the detector after shutdown. The wall is intended to shield the detector from photons generated in the static section of the chamber. This will put emphasis on dose rate caused by the moving block. A CAD model of this geometry was built and the components tagged with material names using Trelis [21].

A neutron source was placed in the central cavity; it was sampled uniformly in space and within the energy interval of 13.8-14.2 MeV. The SDR was measured with a detector after a single pulse irradiation of 1 year and decay period of 30 days. The detector is a sphere, 10cm in radius, located 4.5m in the positive x-direction away from the outer wall of the chamber. The detector material was chosen to be the same as that used in a previous GT-CADIS experiment (52.34 at. % H-1, 47.66 at. % C-12) [3].

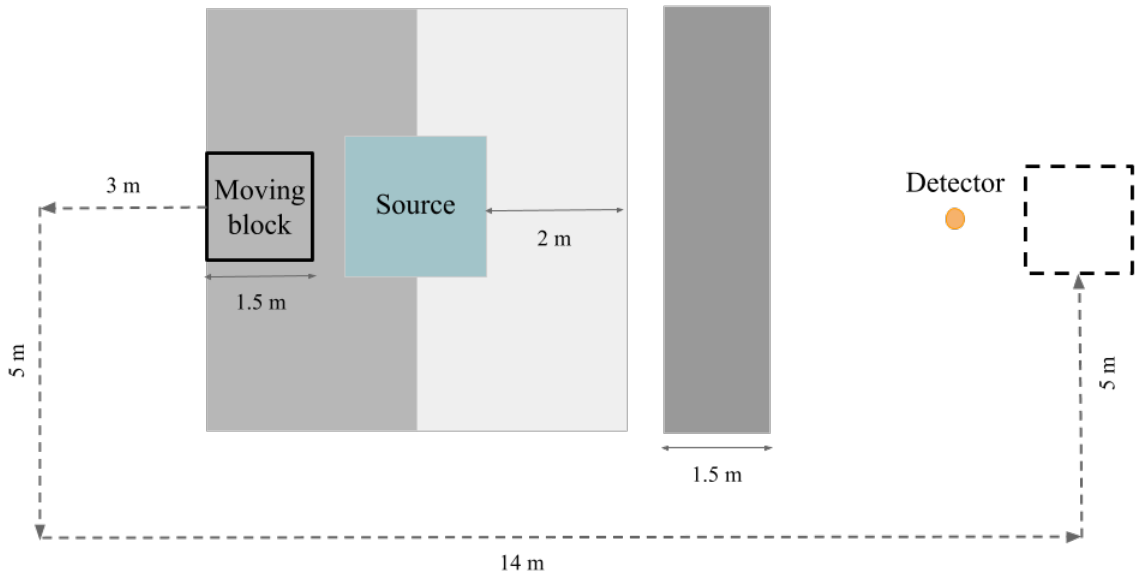

Figure 5.4: Planar view of the geometry. Chamber with 2 m thick walls and central cavity measuring 2 m x 2 m x 2 m and modular block on the left side. Chamber material is a mix of steel and helium. Right half is 15 % steel and left half is 75 % steel by volume. The central cavity is filled with helium and chamber is surrounded by vacuum. A SDR detector is located 4.5 m in the x-direction from the chamber.

First, the VR parameters for both FW-CADIS and TGT-CADIS were generated. Next, the three types of simulations (analog, FW-CADIS, and TGT-CADIS) were performed for varying lengths of processor time: 100 min, 1,000 min, and 10,000 min. Trial and error was used to estimate the number of particles required for each processor time. An estimation of the SDR and FOM were calculated at each time step.

5.5.2 Variance Reduction Parameters

5.5.2.1 FW-CADIS

The AutomateD VAriaNce reducTion Generator (ADVANTG) code [26] was used to produce FW-CADIS VR parameters. First, a forward deterministic transport

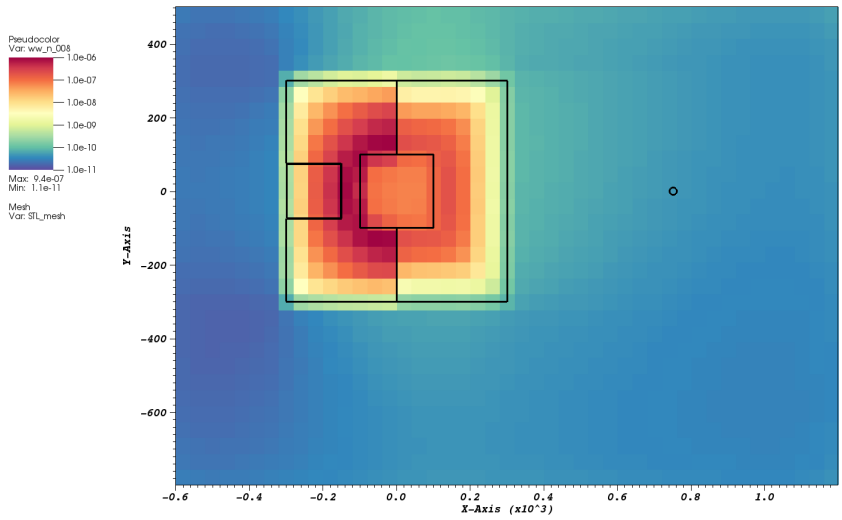

Figure 5.5: Neutron weight windows for the 13.8-14.2 MeV energy group generated by the FW-CADIS method.

simulation is performed via Denovo to get an estimate of the the forward neutron flux. This neutron flux is used to generate the adjoint neutron source via Eq. 2.18. Another deterministic transport simulation is performed to calculate the adjoint neutron flux which is then used to generate VR parameters via the CADIS method. The resulting weight window mesh is shown in Fig. 5.5.

5.5.2.2 TGT-CADIS

The first step of the TGT-CADIS process is calculating the adjoint photon flux at each time step. The ICRP-74 [25] flux-to-dose rate conversion factors define the source at the detector location. The adjoint flux at each time step is shown in Fig. 5.6.

The next step is mapping the values from the global voxel mesh to a tetrahedral mesh that conforms to the geometry at each step. The adjoint flux values are averaged over all of the time steps and mapped onto a a mesh conforming to the original configuration of the geometry. This average adjoint photon flux mesh is shown in

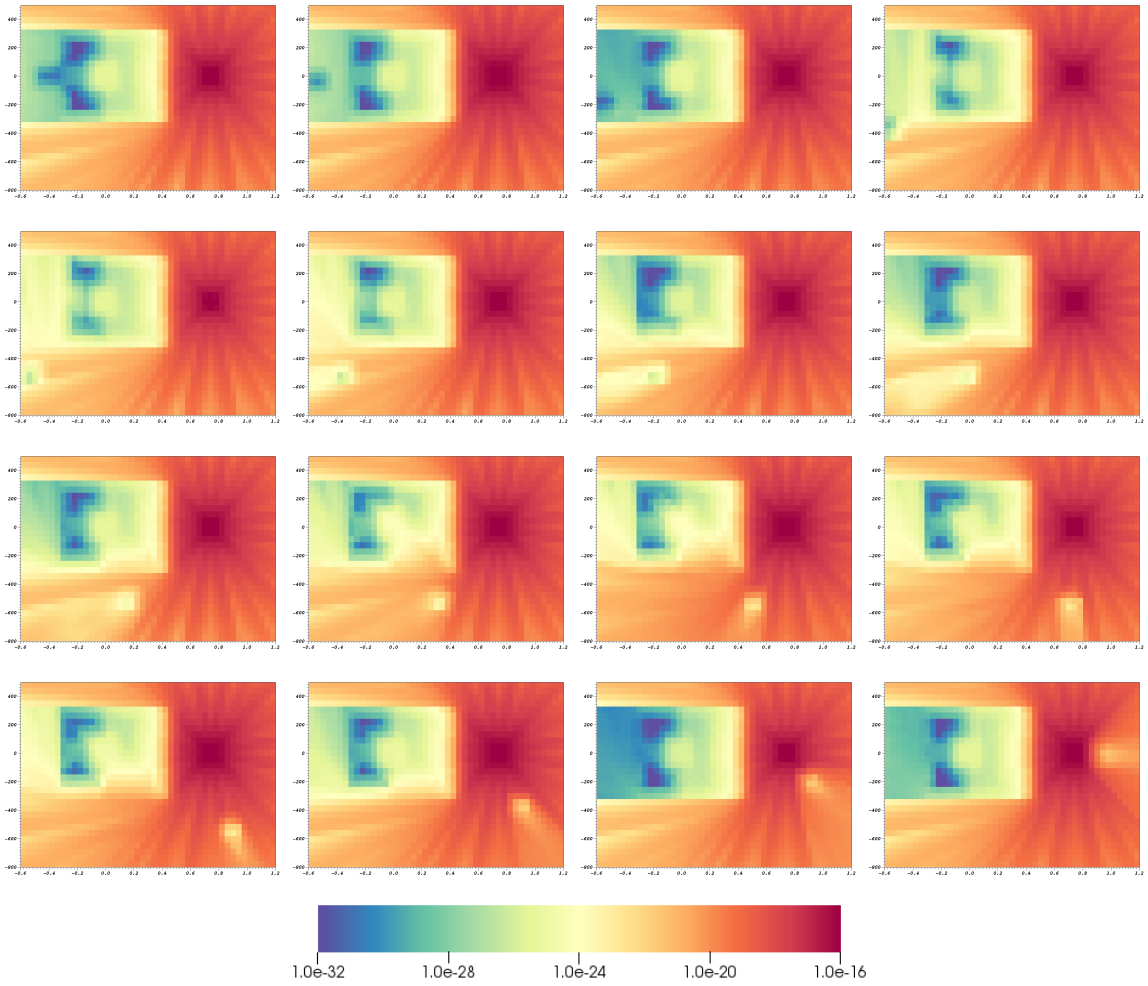

Figure 5.6: Adjoint photon flux [$Sv/photon$] in the 0.8 to 1 MeV group at each time step of geometry movement.

Fig. 5.7 The top to bottom asymmetry in the average adjoint flux in the chamber is caused by the path of the moving block. As seen in the step-wise adjoint photon flux maps in Fig. 5.6, when the block is traveling under the static chamber, photons reflect off of the block, causing a higher adjoint flux in the bottom right side.

The average adjoint photon flux is combined with the T matrix to generate the adjoint neutron source shown in Fig. 5.8. The source is on a voxel mesh which is required by PARTISN. The resulting adjoint neutron flux is shown in Fig. 5.9.

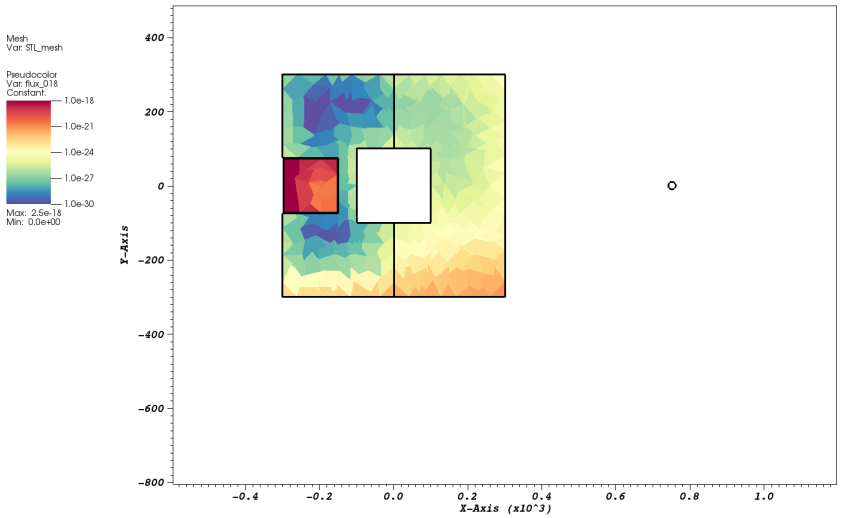

Figure 5.7: Average adjoint photon flux [$Sv/photon$] mapped onto a mesh conforming to the original configuration of the geometry.

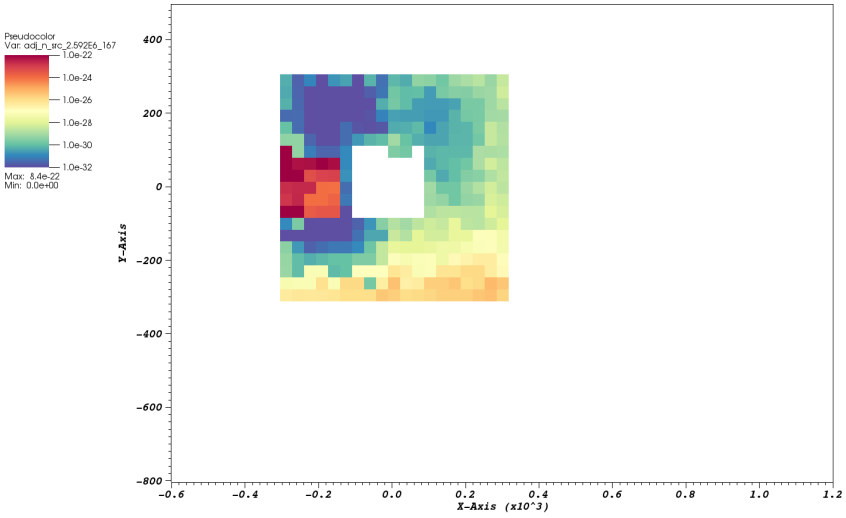

Figure 5.8: Adjoint neutron source [$Sv/(neutron \cdot cm)$] in the 13.8 to 14.2 MeV energy group.

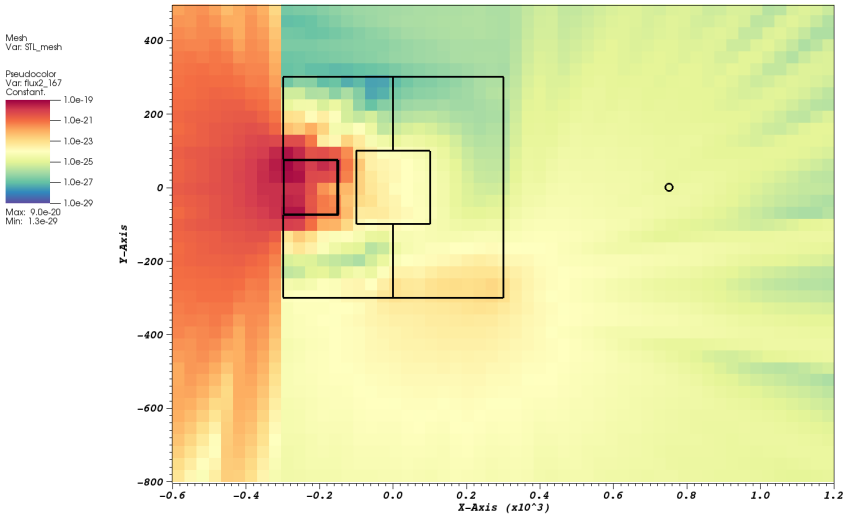

Figure 5.9: Adjoint neutron flux [$Sv/neutron$] in the 13.8 to 14.2 MeV energy group.

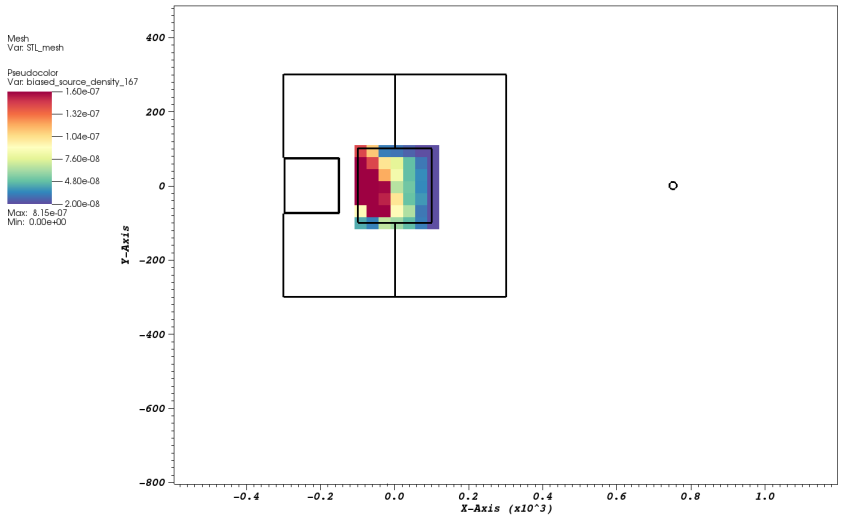

Figure 5.10: Biased neutron source for the 13.8-14.2 MeV energy group generated by the TGT-CADIS method.

The adjoint neutron flux was used to produce the biased source and weight windows shown in Figs. 5.10, 5.11.

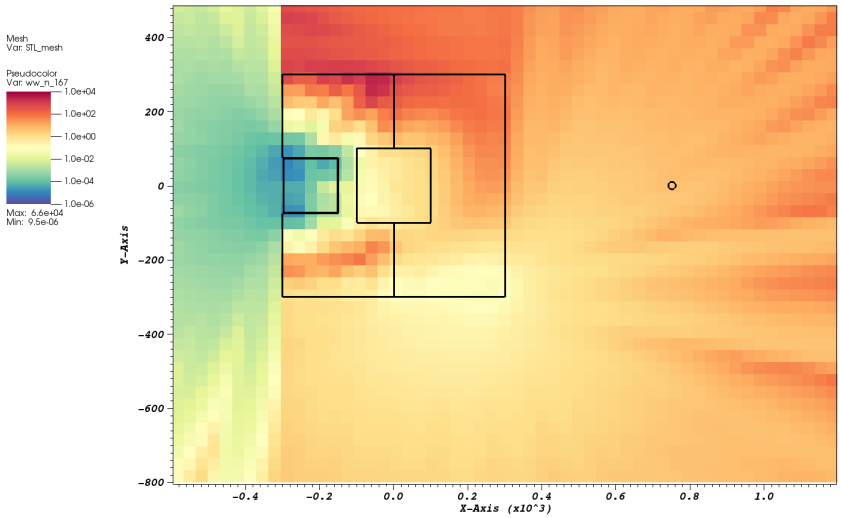

Figure 5.11: Neutron weight windows for the 13.8-14.2 MeV energy group generated by the TGT-CADIS method.

5.5.3 Error in Neutron Flux

The relative error in the neutron flux from each type of simulation for each processor time is shown in Table 5.1. The color bar shows values from 0 to 20% relative error, with a midpoint at 10% error. As stated by the MCNP manual, any tally with relative error less than 10%, blue in this case, is generally reliable [5].

As expected, the error decreases with increasing processor time in all cases. Recall that FW-CADIS has the goal of uniformly reducing error across the entire mesh tally while TGT-CADIS has the goal of reducing the error in the regions that will produce photons that contribute to the final SDR. From the importance map shown in Fig. 5.9, it can be seen that the moving block and bottom right side of the chamber are important to the SDR. Therefore, the TGT-CADIS method aims to reduce the error in these regions. Comparing the error in the 1,000 minute simulation time, the TGT-CADIS method has reduced the error in these important regions to less than 10%, whereas in the other two methods, mesh elements with

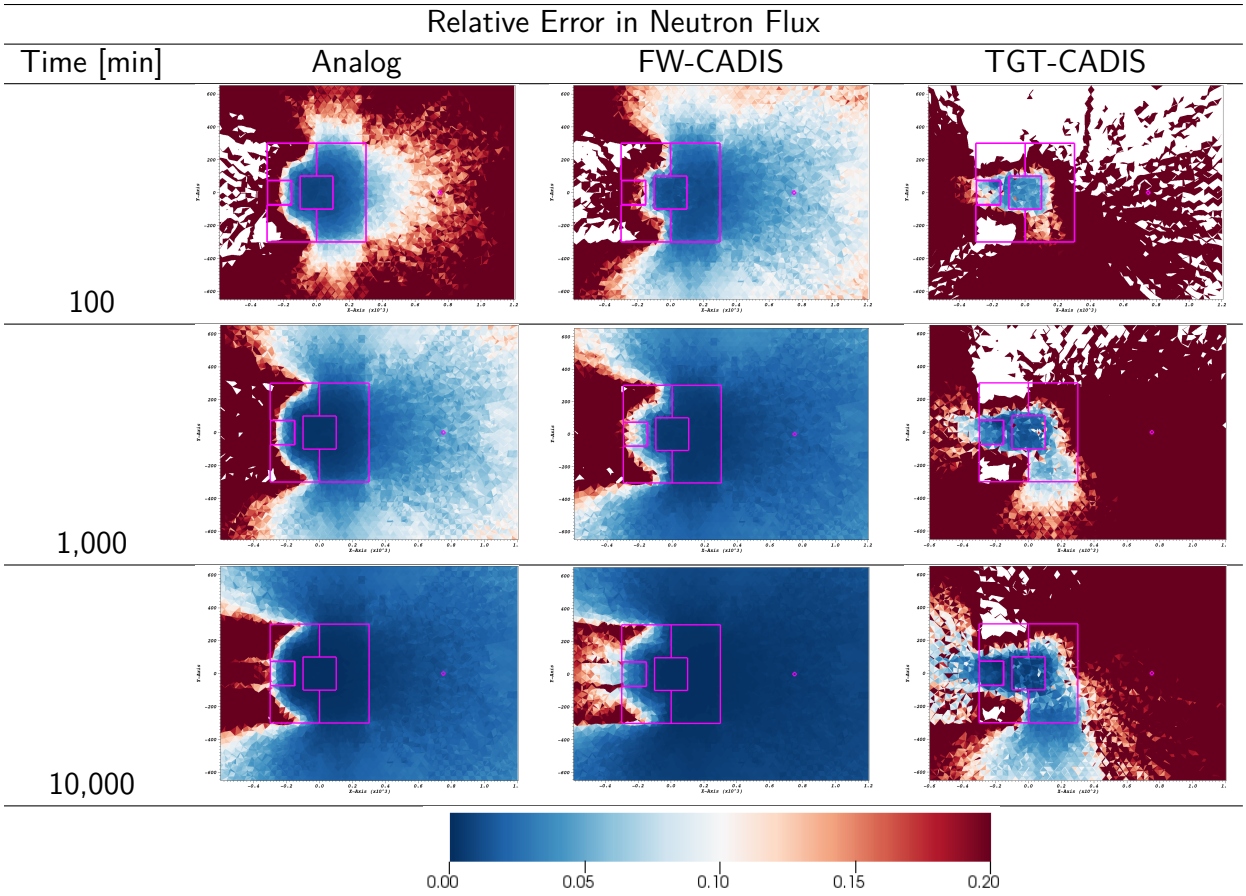

Table 5.1: Error in total neutron flux for analog, FW-CADIS, and TGT-CADIS neutron transport performed at three different processor times.

error above 10% still remain.

5.5.4 Estimation of SDR

Traditionally, the SDR is calculated directly by the MC code by modifying a flux tally with flux-to-dose rate conversion factors. The error in SDR calculated in this manner is strictly statistical error from the photon transport simulation. In order to capture the error in the SDR resulting from the neutron transport calculation, the SDR at the detector location can be estimated using Eq. 2.12. It is written in discrete

form in Eq. 5.16:

$$SDR_t = \sum_{\nu} \sum_{h} \Psi^{+}_{\gamma,h,\nu,t} \cdot q_{\gamma,h,\nu,t} \cdot V_\nu \tag{5.16}$$

where V_ν is the volume of element ν, $\Psi^{+}_{\gamma,h,\nu,t}$ is the adjoint photon flux, and $q_{\gamma,h,\nu,t}$ is the forward photon source in energy group h, volume element, ν, at time step t. The contribution to the SDR from each volume element is then given by Eq. 5.17:

$$SDR_{\nu,t} = \sum_{h} \Psi^{+}_{\gamma,h,\nu,t} \cdot q_{\gamma,h,\nu,t} \cdot V_\nu. \tag{5.17}$$

The adjoint photon flux at each time step was previously calculated in the first step of the TGT-CADIS process. The forward photon source can be estimated by Eq. 5.18:

$$q_{\gamma,h,\nu,t} = \sum_{g} T_{g,h,\nu,t} \cdot \phi_{n,g,\nu}. \tag{5.18}$$

The forward photon source is a function of neutron flux, therefore, the error in the estimate of SDR due to neutron transport derives from the error in forward source:

$$\sigma^2_{q_{\gamma,h,\nu,t}} = \sum_{g} \left(T_{g,h,\nu,t} \cdot \sigma_{\phi_{n,g,\nu}} \right)^2. \tag{5.19}$$

The error in the SDR at each time step is then given by Eq. 5.20:

$$\sigma^2_{SDR_t} = \sum_{\nu} \sum_{h} \left(\Psi^{+}_{\gamma,h,\nu,t} \cdot \sigma_{q_{\gamma,h,\nu,t}} \cdot V_\nu \right)^2. \tag{5.20}$$

The estimated SDR at the detector location at each time step for each processing time is shown in Figs. 5.12, 5.13, and 5.14. The SDR at the detector reaches a peak value at time step 14. A map of the contribution to the SDR, calculated by Eq. 5.17, and the associated relative error at this time step is shown for each simulation type,

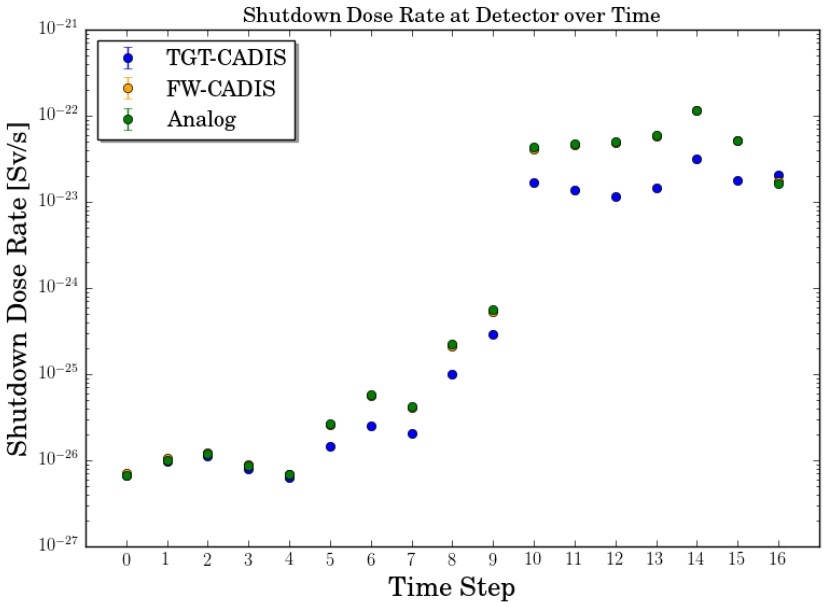

Figure 5.12: Estimate of the SDR calculated by each simulation method for 100 minutes of processing time.

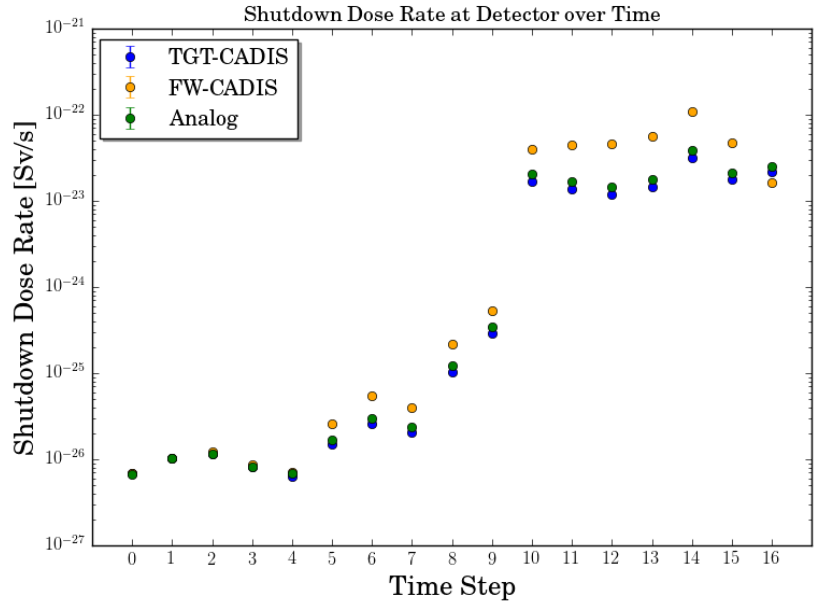

Figure 5.13: Estimate of the SDR calculated by each simulation method for 1,000 minutes of processing time.

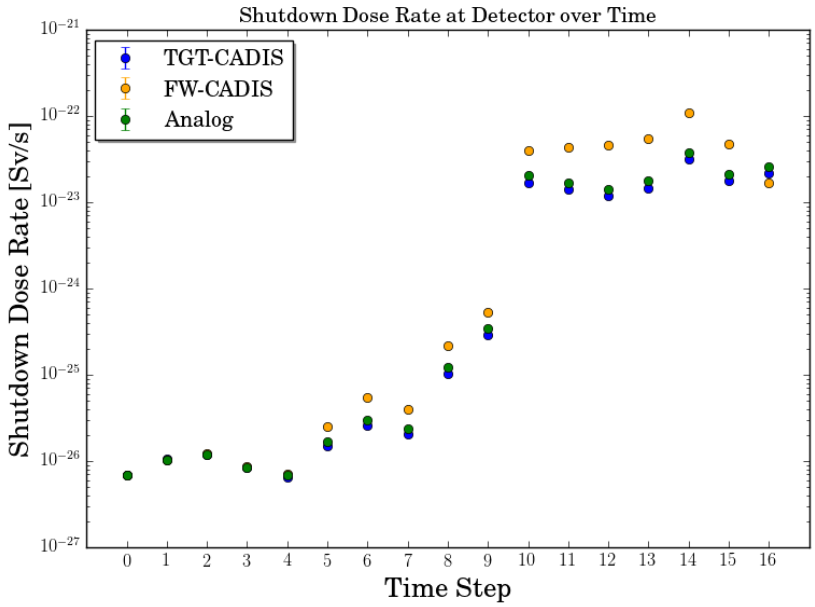

Figure 5.14: Estimate of the SDR calculated by each simulation method for 10,000 minutes of processing time.

at 100, 1,000, and 10,000 minutes of computer time, in Tables 5.2, 5.3, and 5.4.

The activated moving block is the largest contributor to the SDR at this time step and the error in the block is lowest in the TGT-CADIS simulations. Comparing the results from the 1,000 minute simulation in Table 5.3, it can be seen that all elements in the moving block in the TGT-CADIS simulation have error below 10%, while elements with error above 10% still exist in both the analog and FW-CADIS simulations.

The FOM was calculated using Eq. 2.2. The results for each processing time are shown in Figs. 5.15, 5.16, and 5.17. The TGT-CADIS method has a higher FOM for most time steps after the block moves beyond the shielding effect of the static chamber and becomes a more important contributor to the SDR. The higher FOM is largely due to the lower error in the regions of greatest importance, the moving block and the bottom right section of the static chamber.

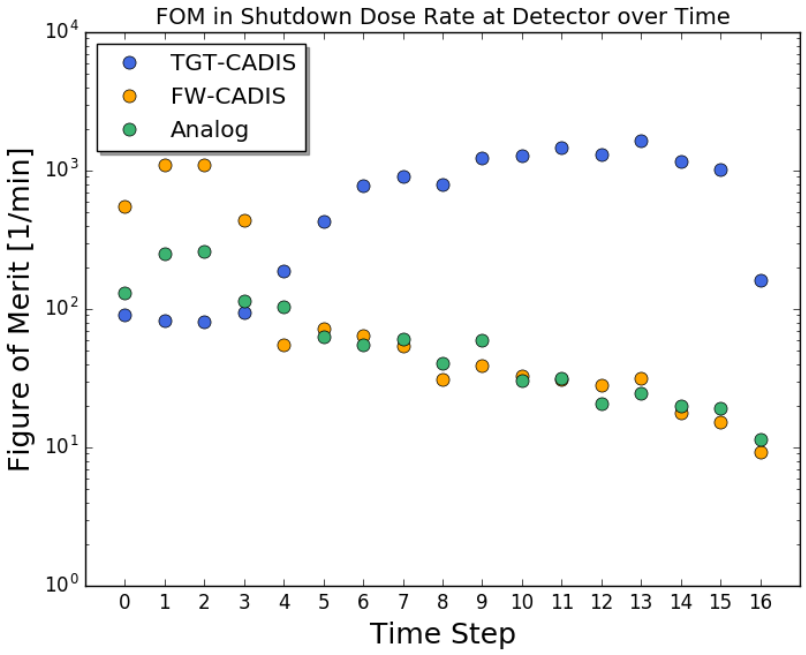

Figure 5.15: FOM for each simulation method for 100 minutes of processing time.

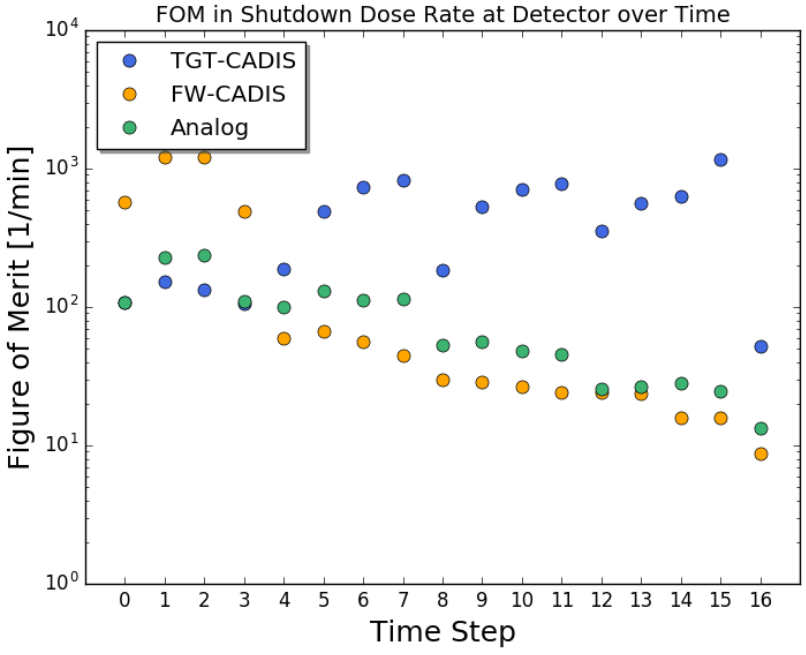

Figure 5.16: FOM for each simulation method for 1,000 minutes of processing time.

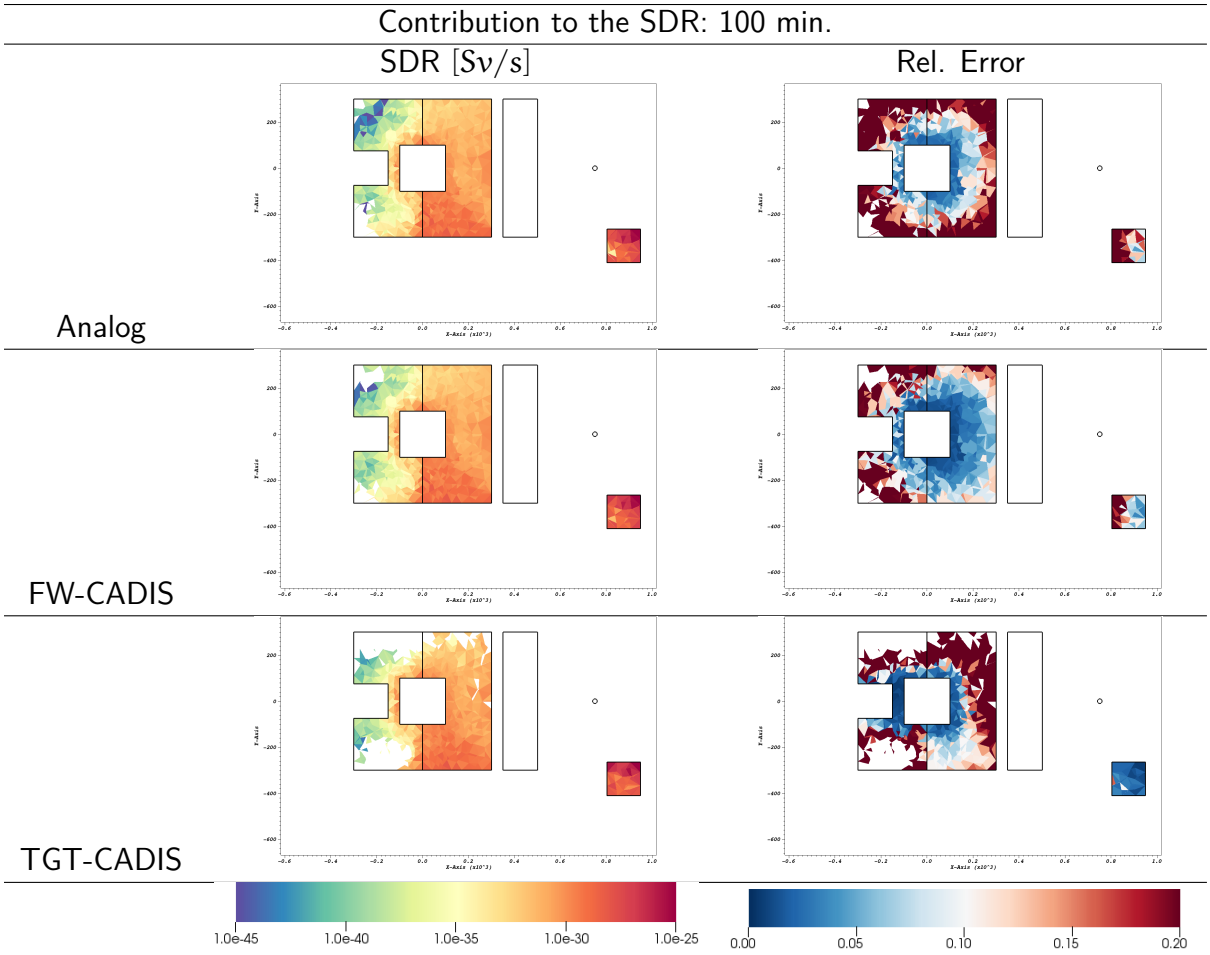

Table 5.2: Contribution to the SDR and the associated relative error for each simulation method. Each was run for 100 minutes of computer time.

Comparing the FOM in the TGT-CADIS method across all computer times, it appears to decrease in the simulation that was run for 10,000 minutes. To investigate this further, the frequency of squared absolute error values in the SDR for a single time-step is shown in Fig. 5.18. As processing time increases, the expected trend of less elements with higher error and more elements with lower error can be seen. To align the data with the 10,000 minute simulation for a closer comparison, the the 100 minute simulation results were divided by 100 and the the 1,000 minute simulation results were divided by 10 in Fig. 5.19. This closer comparison reveals a single

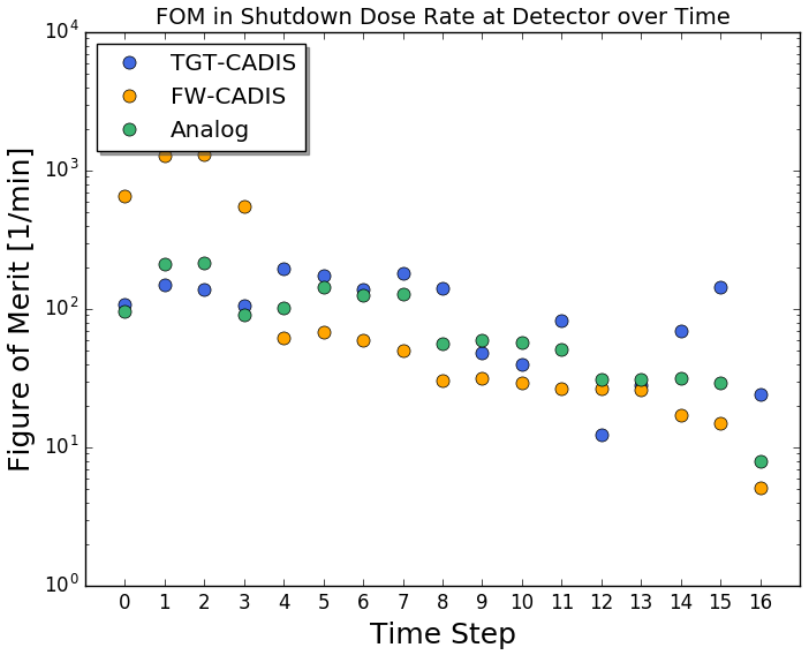

Figure 5.17: FOM for each simulation method for 10,000 minutes of processing time.

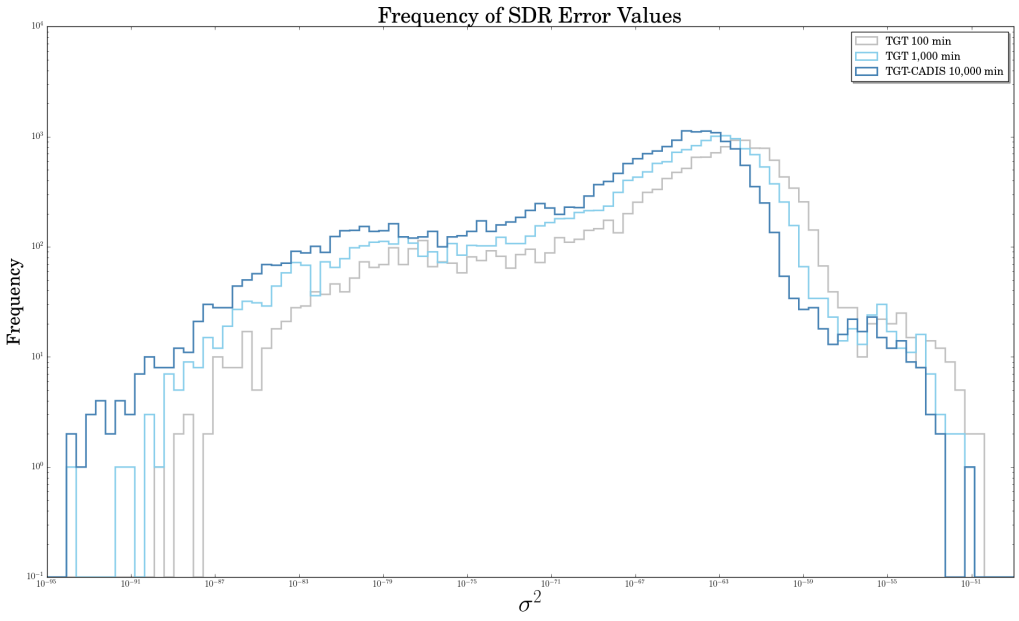

Figure 5.18: Frequency of SDR error values at each computer time.

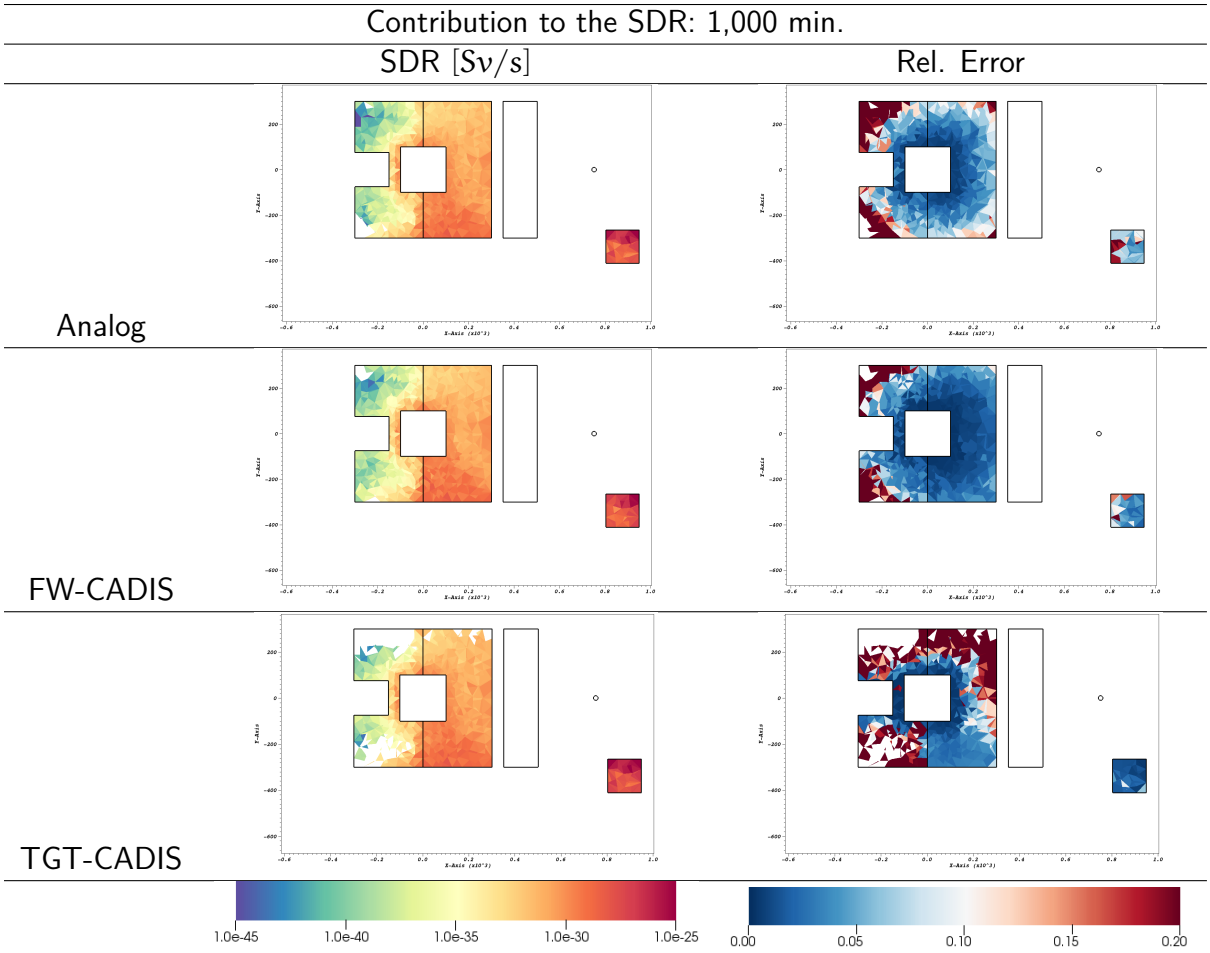

Table 5.3: Contribution to the SDR and the associated relative error for each simulation method. Each was run for 1,000 minutes of computer time.

element in the 10,000 minute simulation with error two orders of magnitude higher than the next highest error. The equation for FOM can be written as a function of the squared absolute error in SDR:

$$\text{FOM} = \frac{\text{SDR}^2}{\sigma^2_{\text{SDR}} \cdot t_{\text{proc}}}. \tag{5.21}$$

From this equation, it is clear that a single high-error element can greatly reduce the FOM.

Contribution to the SDR: 10,000 min.		
	SDR $[Sv/s]$	Rel. Error
Analog	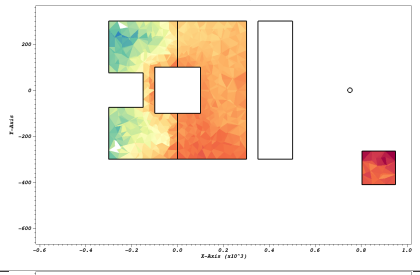	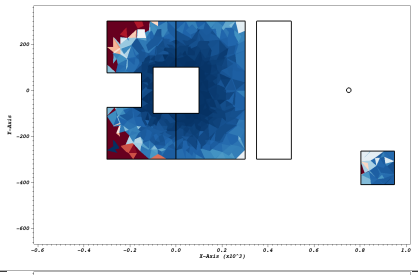
FW-CADIS	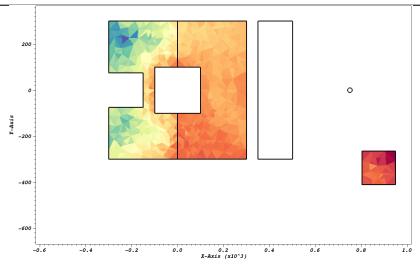	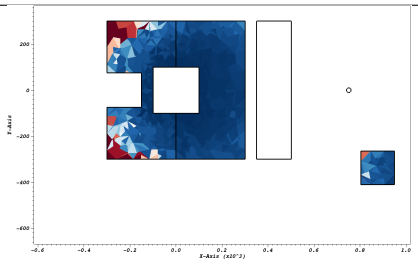
TGT-CADIS	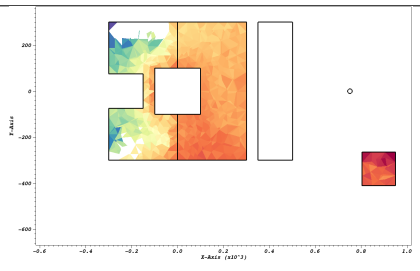	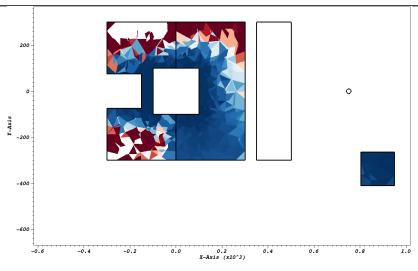
	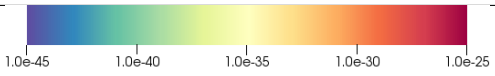	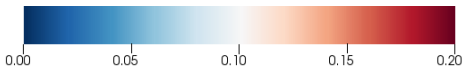

Table 5.4: Contribution to the SDR and the associated relative error for each simulation method. Each was run for 10,000 minutes of computer time.

The FOM for the 10,000 minute TGT-CADIS simulation was adjusted by removing the single high-error element. The adjusted FOM is shown in Fig. 5.20. The adjusted FOM plot shows a trend of higher FOM for the TGT-CADIS method for most time steps after the moving block becomes the dominating contributor to the SDR.

The difference in magnitude of the curves in Fig. 5.19 can be attributed to scoring in additional elements with increasing run time. This effect can also be seen in Table 5.5 that compares the contributions to the SDR and the associated relative error for the TGT-CADIS method at each processing time. Comparing the relative error

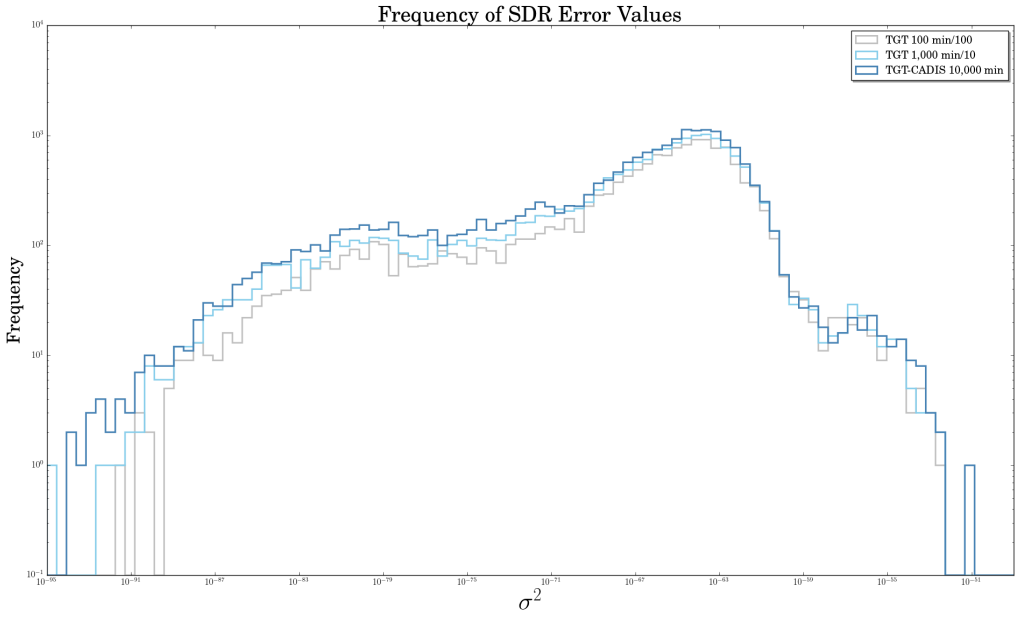

Figure 5.19: Comparison of the frequency of SDR error values. There is a single element in the 10,000 minute simulation with error two orders of magnitude higher than the next highest error.

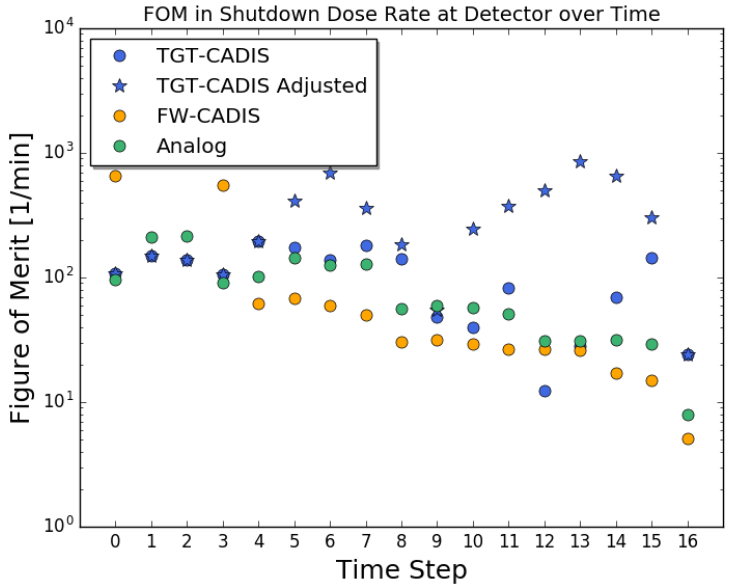

Figure 5.20: Adjusted FOM for TGT-CADIS simulation added to comparison of FOM for 10,000 minutes of processing time.

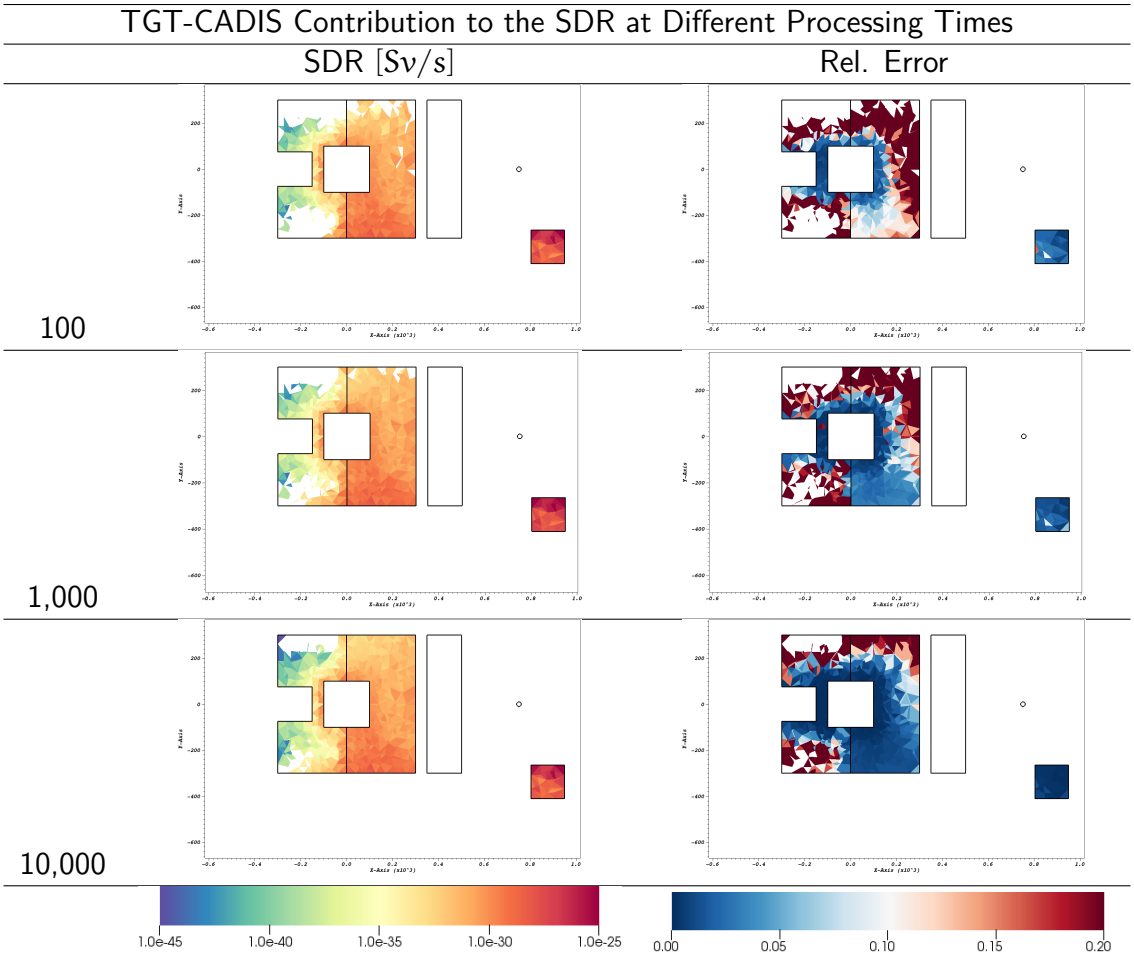

Table 5.5: Contribution to the SDR and the associated relative error generated by the TGT-CADIS method for each processing time.

results, it can be seen that with increasing processor time, some elements in the top right corner of the chamber progress from no result in the 100 and 1,000 minute simulations to a result with high error in the 10,000 min simulation.

The FOM for the total accumulated dose was also calculated for each simulation type. The results are shown in Table 5.6. The FOM for total accumulated dose is higher for the TGT-CADIS method than both analog and FW-CADIS.

	FOM Total Accumulated Dose		
Time [min]	Analog	FW-CADIS	**TGT-CADIS**
100	301.38	286.21	**9342.01**
1,000	397.18	254.82	**3341.11**
10,000	348.33	266.83	**642.30**
10,000			**1766.21***

Table 5.6: Comparison of FOM in total accumulated dose across all simulation methods and all processing times. *FOM adjusted by removing high error element.

5.6 Effect of Time Step Discretization

The number of time steps chosen determines the degree of accuracy to which the average adjoint photon flux map represents the actual behavior of the moving geometry. If too few time steps are chosen, important features of the adjoint photon flux map can be missed which could lead to non-optimal VR parameters.

To demonstrate this effect, different numbers of time steps were chosen. First, only two steps, the original and final positions, were averaged together.Next, three and seven intermediate positions were averaged together with the original and final positions. Results are shown in Fig. 5.21. If only two positions, original and final, were chosen, the importance of the bottom right side of the chamber would be missed. When intermediate steps are taken into account, the average behavior of the moving block is more accurately captured. The lower right side of the chamber is important because during the time that the moving block is moving past it, photons from this region reflect off of the block and contribute to the dose at the detector.

5.7 Summary

In this chapter, the TGT-CADIS adjoint neutron source was derived and the implementation of the VR method was described. TGT-CADIS was then applied to a

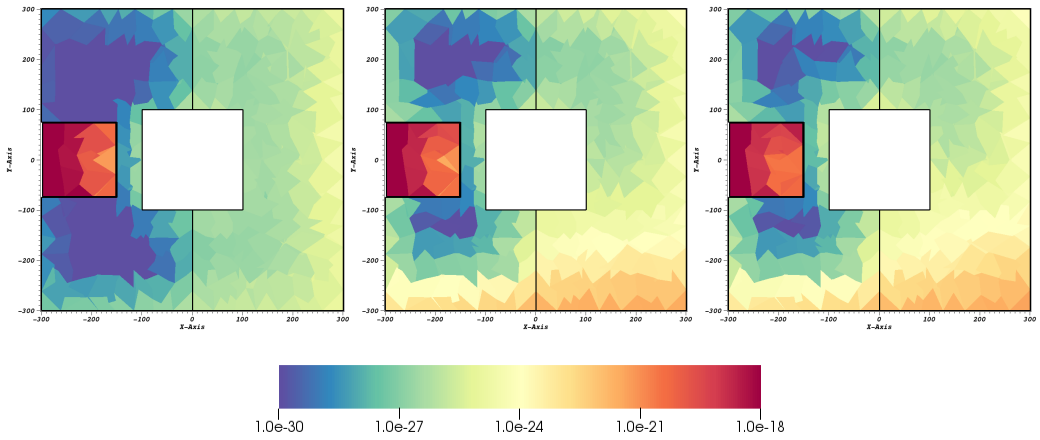

Figure 5.21: Average adjoint photon flux [$Sv/photon$] in 0.8 to 1.0 MeV group with (left to right) two, five, and nine time steps.

simple problem and compared to simulations run in analog and using FW-CADIS for optimization. It was found that the TGT-CADIS method efficiently reduces error in the regions important to the final SDR. The FOM in the total accumulated dose calculation was higher for TGT-CADIS than both analog and FW-CADIS. Future work is needed to determine the significance of the under-sampling in the top right section of the static chamber and the cause of the single high-error element.

Chapter 6

Production-level Demonstration

The TR2S and TGT-CADIS methods have been described and demonstrated on simplified demonstration problems in the previous chapters. In this chapter, both methods will be applied to a production-level model to produce optimized, time-dependent SDR maps.

6.1 Problem Description

The model chosen for this demonstration is a simplified version of the 1 m Princeton Plasma Physics Laboratory (PPPL) Spherical Tokamak (ST) Fusion Nuclear Science Facility (FNSF) device. It was previously used in the original demonstration of the GT-CADIS method [28] where a thorough description of the model, materials, and source are also given. This model only contains the components inside the vacuum vessel and some components and materials are homogenized for simplicity. Even with simplifications, this is still a relatively large, complex geometry, so a single octant of the geometry with reflective boundaries was used in this simulation. A 3D view of the CAD model and a legend of materials is shown in Fig. 6.1.

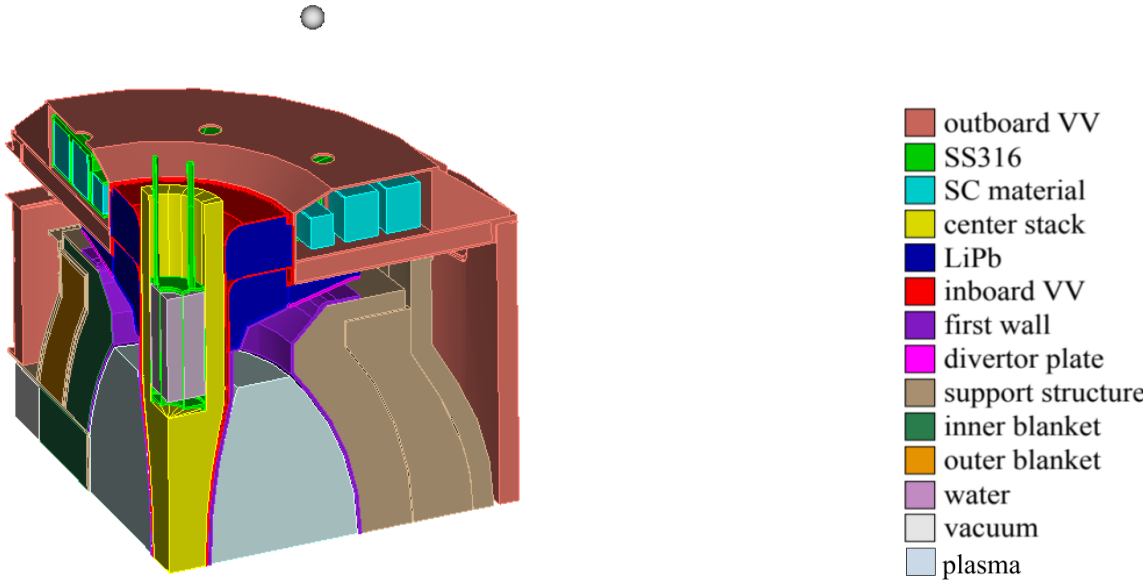

Figure 6.1: 3D view of an octant model of the 1 m PPPL ST-FNSF device and material legend. "VV" is vacuum vessel and "SC" is superconducting.

This model contains modular ports in which experimental material can be placed. To demonstrate the TGT-CADIS and TR2S capabilities, one of the ports was moved out of the device and upwards past a photon detector. The path of movement is shown in Fig. 6.2. This path was discretized into six steps including the original configuration.

The mesh-based plasma neutron source was generated using DAGMC plasma source capabilities that allow for random sampling of initial positions and energies. A 50° slice of the source density for the 13.8-14.2 MeV energy group is shown in Fig. 6.3. A simple, single pulse 2 year irradiation and 30 day decay scenario was chosen.

DAG-MCNP5 was used for forward radiation transport and PARTISN was used for adjoint transport simulations. ALARA with FENDL-2.0 data was used for activation analysis.

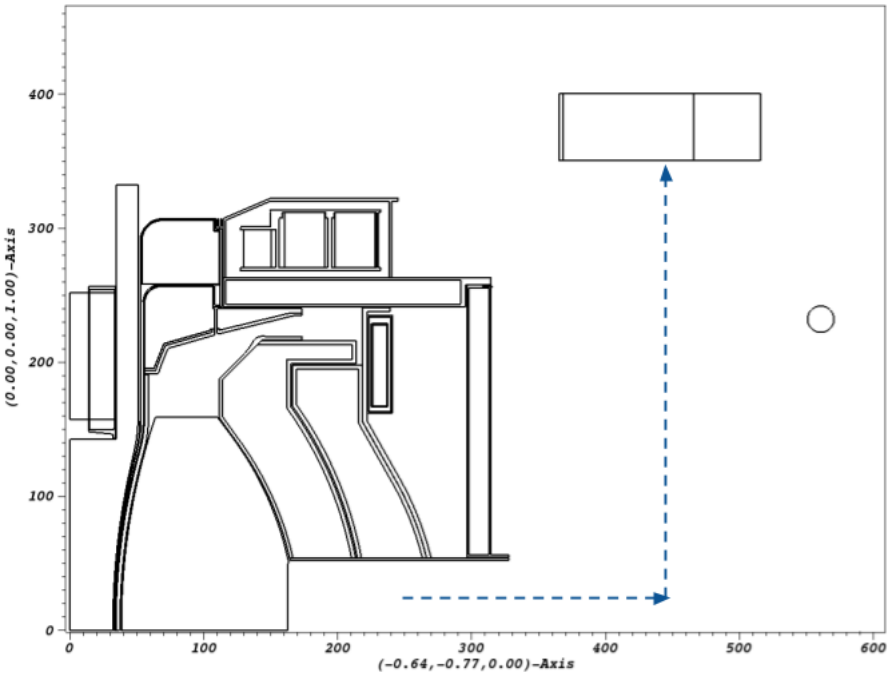

Figure 6.2: Slice of FNSF showing path of experimental port.

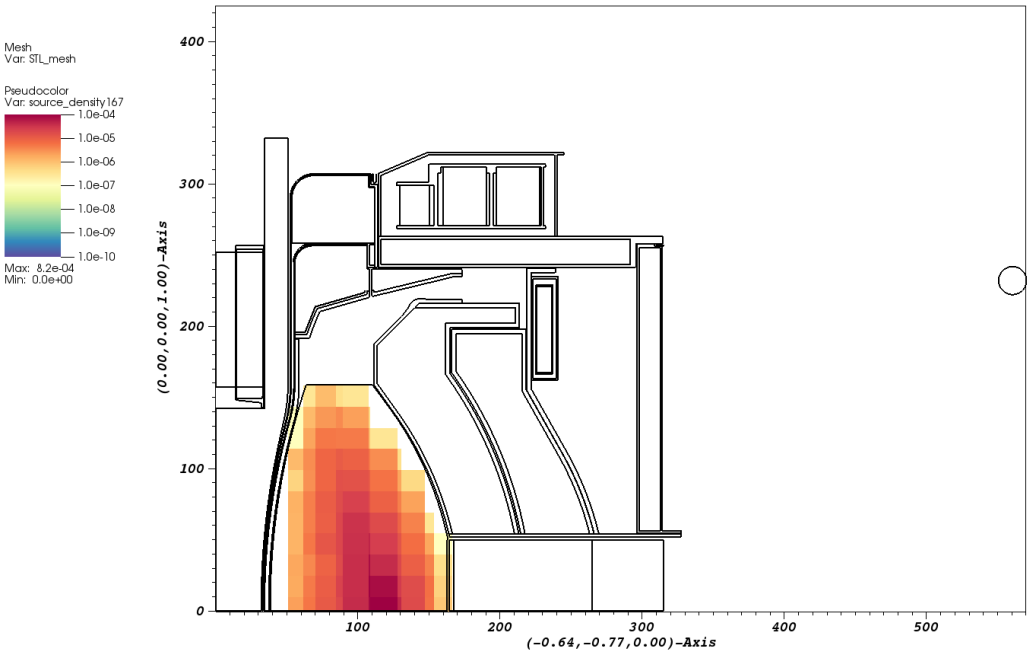

Figure 6.3: Mesh-based neutron source in the 13.8-14.0 MeV energy group.

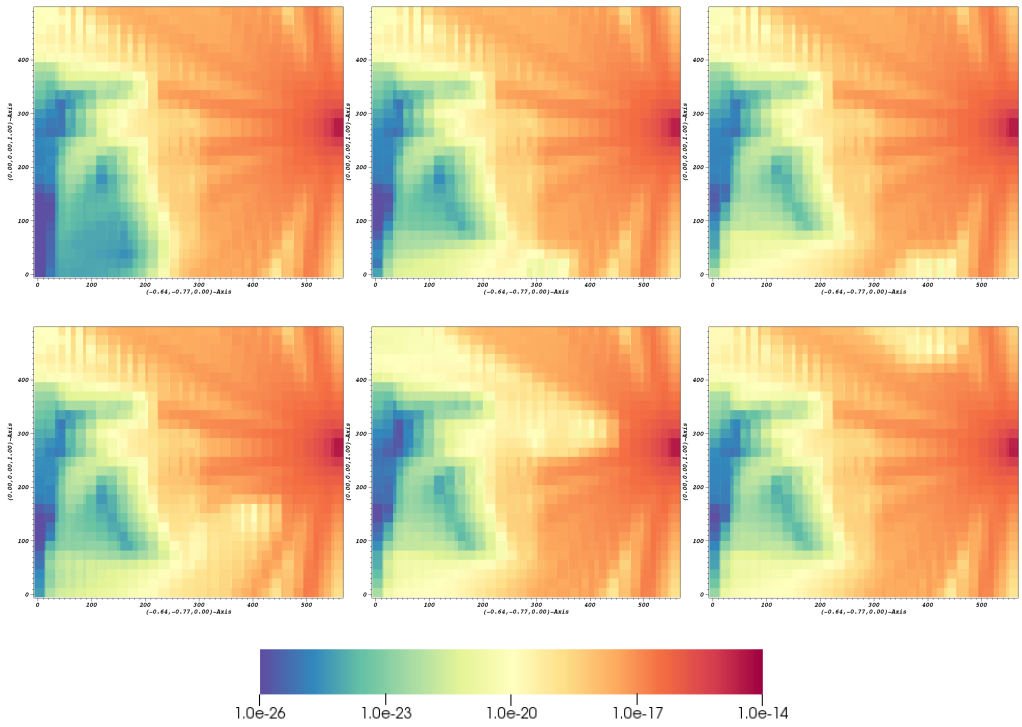

Figure 6.4: Adjoint photon flux [$Sv/photon$] in FNSF in the 0.8-1.0 MeV energy group at each time step of geometry movement.

6.2 TGT-CADIS VR Parameters

This model was previously evaluated and found to adhere to the SNILB criteria so the standard GT-CADIS, and therefore TGT-CADIS, method is appropriate for generating optimal VR parameters.

The first part of the workflow laid out in Chapter 5 is calculating the adjoint photon flux at each step of geometry movement. The results from each time step are shown in Fig. 6.4.

The next step is averaging the adjoint photon flux over all of the time steps and mapping the result onto a conformal mesh of the geometry in the original configuration. The average adjoint flux is shown in Fig. 6.5. This can be compared to the adjoint photon flux map of the geometry in its original configuration in Fig.

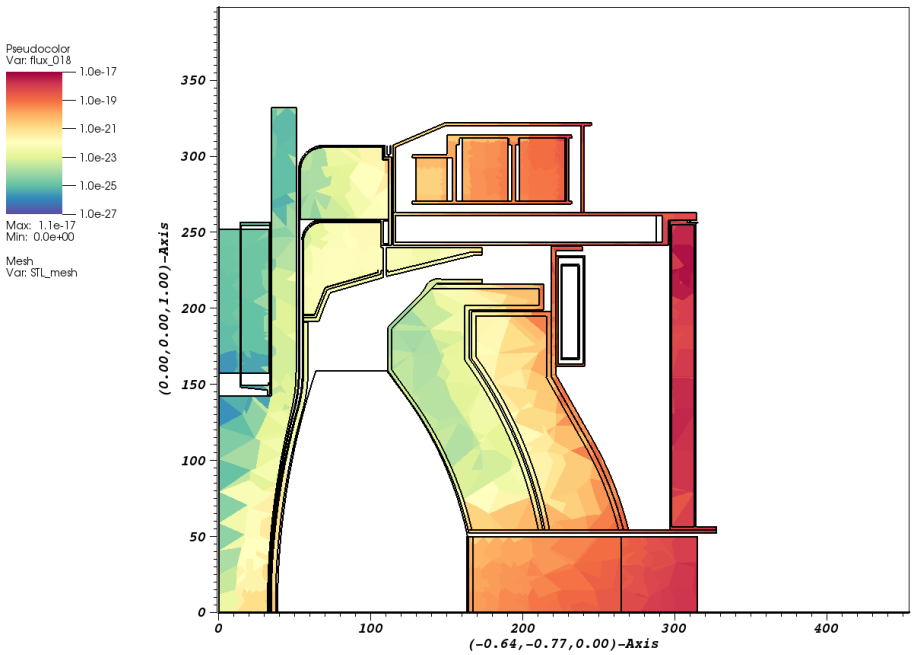

Figure 6.5: Average adjoint photon flux [$Sv/photon$] in FNSF in the 0.8-1.0 MeV energy group.

6.6, which would be used if movement after shutdown was not considered. When movement is taken into account, the adjoint photon flux is higher in both the moving component and inboard components that are no longer shielded from the adjoint source/detector when the experimental port is moved.

Next, the T matrix is calculated and combined with the average adjoint photon flux to generate the adjoint neutron source shown in Fig. 6.7. The resulting adjoint neutron flux is shown in Fig. 6.8.

The adjoint flux is used with the CADIS method to generate the biased source and weight windows shown in Figs. 6.9 and 6.10.

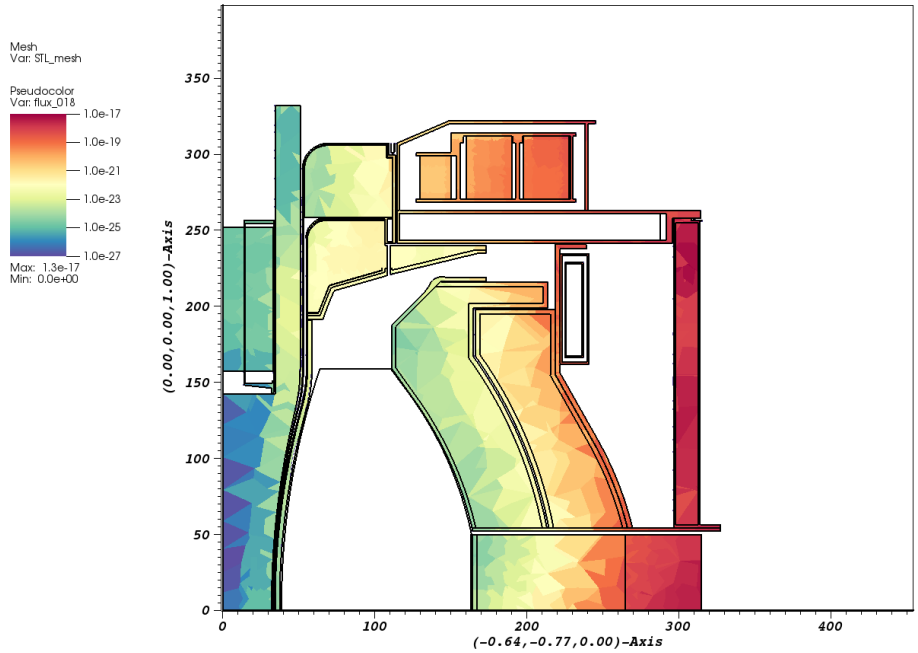

Figure 6.6: Adjoint photon flux [Sv/photon] in the original configuration of FNSF in the 0.8-1.0 MeV energy group.

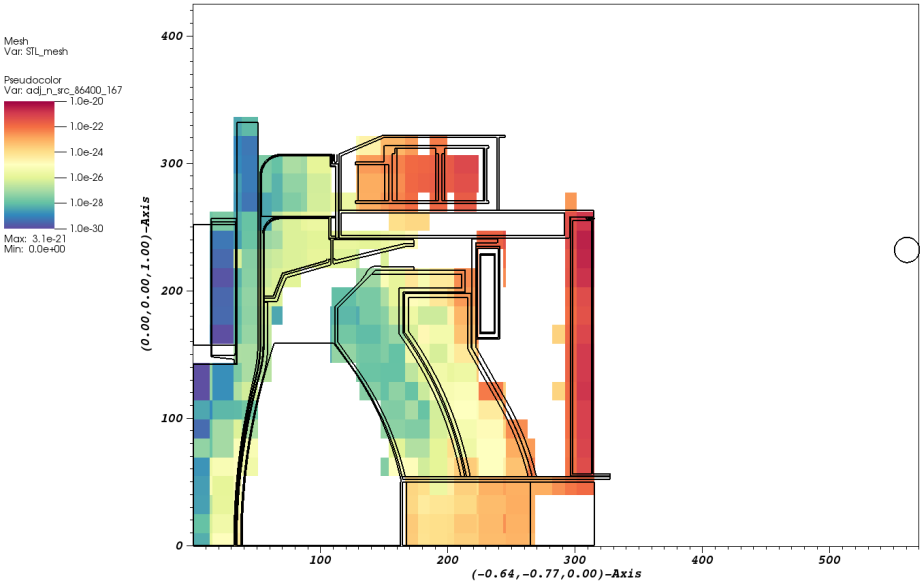

Figure 6.7: Adjoint neutron source [$Sv/(\mathrm{neutron} \cdot \mathrm{cm})$] in FNSF for the 13.8-14.2 MeV energy group.

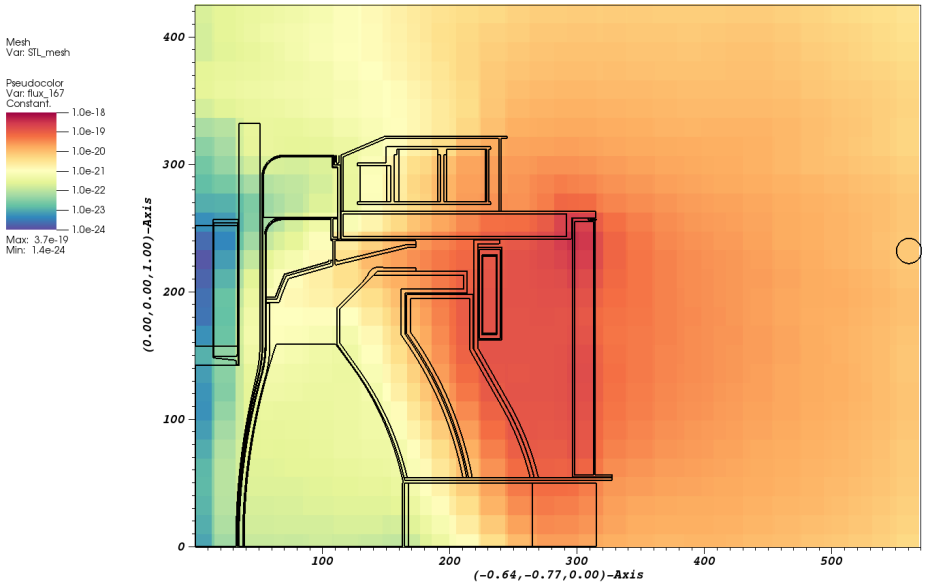

Figure 6.8: Adjoint neutron flux in FNSF for the 13.8-14.2 MeV energy group.

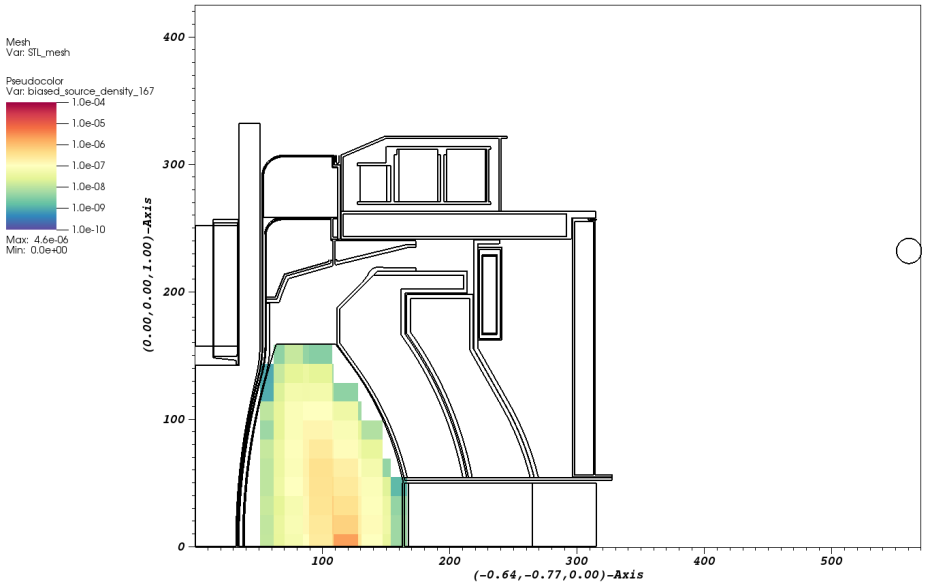

Figure 6.9: FNSF biased neutron source for the 13.8-14.2 MeV energy group.

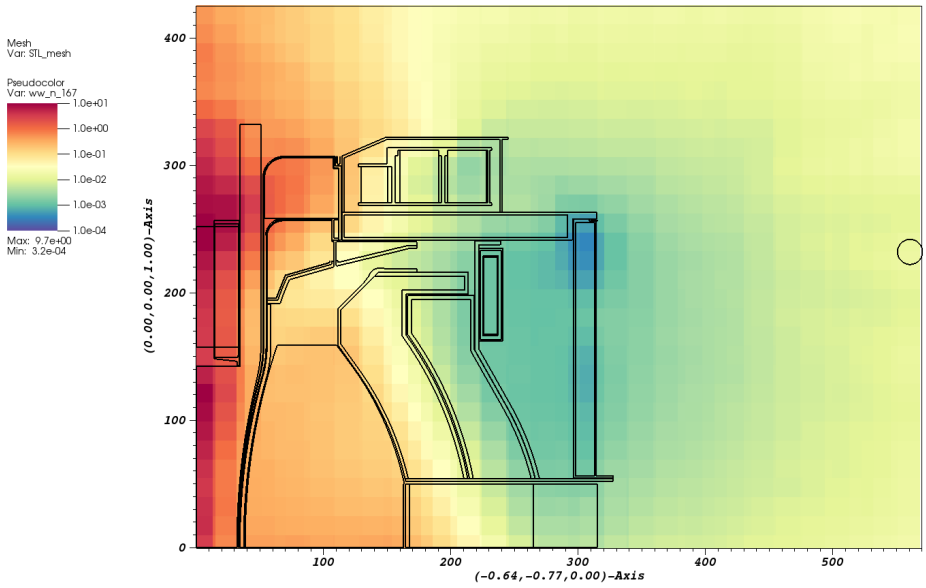

Figure 6.10: FNSF neutron weight windows for the 13.8-14.2 MeV energy group.

6.3 Time-dependent SDR Maps

The biased source and weight windows were used to optimize the forward neutron transport step of TR2S. The resulting neutron flux is shown in Fig. 6.11. To demonstrate the effectiveness of the TGT-CADIS VR parameters, the relative error in the neutron flux is compared to that from an analog simulation in Fig. 6.12. The same number of histories was simulated in both runs. The TGT-CADIS method reduces the error in the outboard VV and the moving experimental port; both of which become activated and contribute to the SDR.

Activation analysis was performed and the resulting photon source is shown in Fig. 6.13. The transform tool was used to move the source and CAD geometry to the appropriate position for each time step of geometry movement. Forward photon transport was performed and the flux tally mesh modified with ICRP-74 flux-to-dose rate conversion factors [25] was used to generate the SDR maps shown in Fig. 6.14.

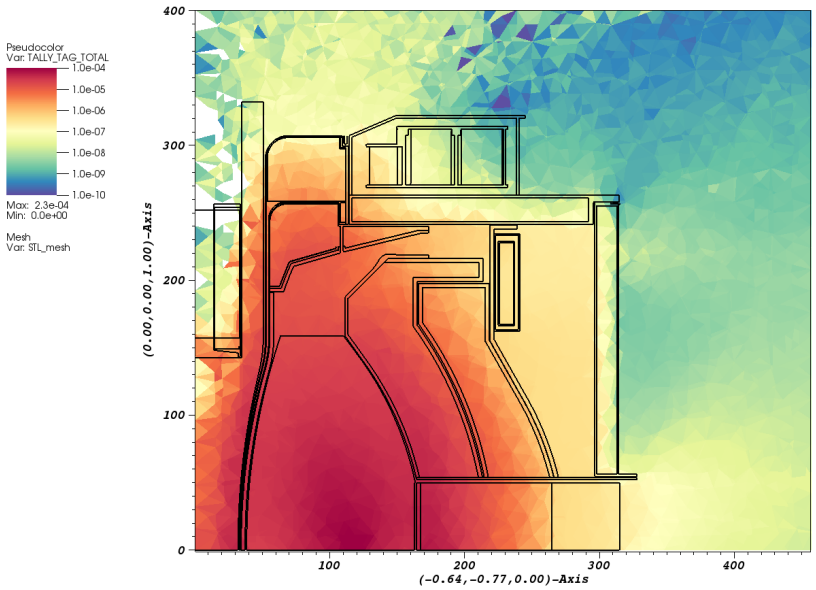

Figure 6.11: Total neutron flux $[neutrons/(cm^2 \cdot s)]$ in FNSF.

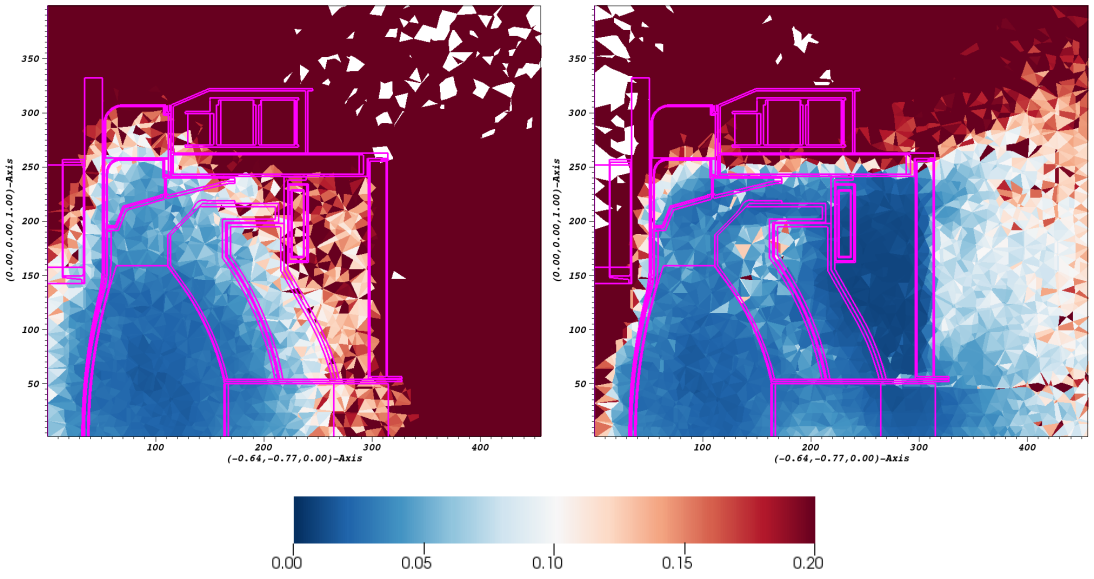

Figure 6.12: Comparison of the relative error in the total neutron flux in FNSF between an analog (left) TGT-CADIS (right) simulation.

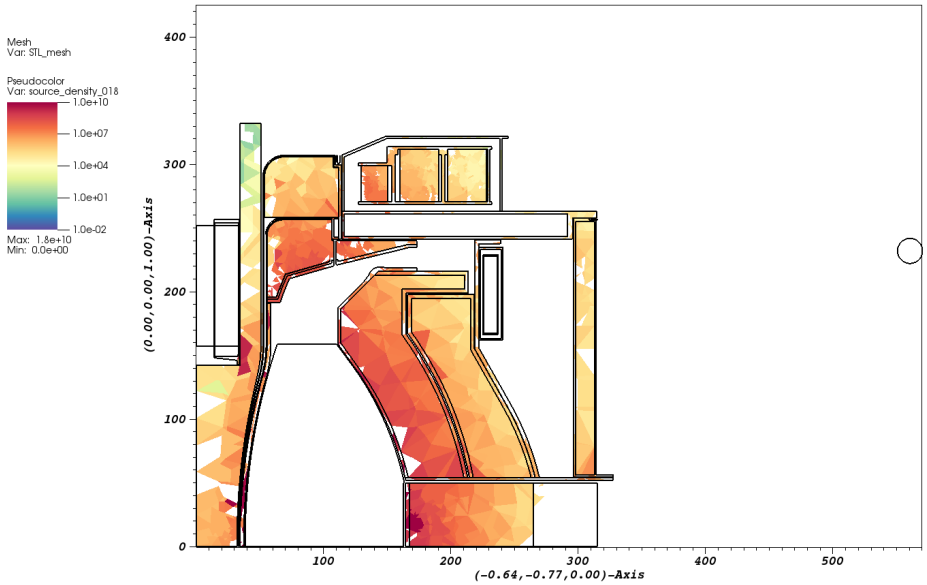

Figure 6.13: Photon source [$photons/(cm^3 \cdot s)$] in the 0.8 to 1.0 MeV group in FNSF.

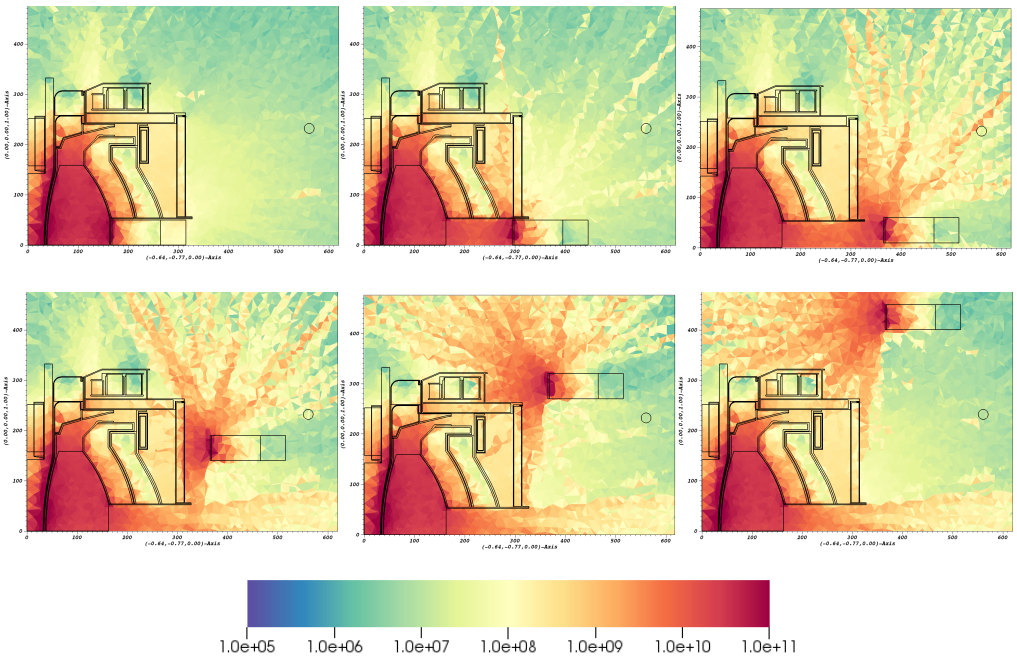

Figure 6.14: SDR [pSv/s] in FNSF at each time step of geometry movement.

As the activated port moves outwards and upwards towards the detector, the dose rate at the detector location increases. Photon transport was run in analog, but the CADIS method could be used to generate VR parameters for each time step.

6.4 Summary

In this chapter, the TGT-CADIS method was applied to a production-level problem. The transformation tool was used to move an experimental port out of its original position and upwards past a SDR detector. The TGT-CADIS method produced VR parameters that when compared to analog, effectively reduced the error in the neutron flux in the experimental port, an important region according to the adjoint neutron flux map. The TR2S method was then used to produce time-dependent SDR maps. In the future, increasing the time-step discretization and using CADIS to optimize photon transport will produce a more finely resolved estimation of the SDR at the detector location over time.

Chapter 7

Summary and Future Work

The MC method is the most accurate way to obtain detailed distributions of the neutron and photon fluxes in FES. In most cases, it is necessary to use VR methods to efficiently calculate these results. The GT-CADIS method, the implementation of MS-CADIS specifically for SDR analysis, has been proven to effectively optimize the neutron transport step of SDR calculations in static systems.

In the case of geometry movement after shutdown, the importance of the photons to the detector SDR changes over time. This requires an extension to GT-CADIS that takes the movement into account. In this work, the TGT-CADIS method was developed to generate a time-integrated adjoint neutron source term. This term ultimately aims to reduce the error in the neutron transport simulation of systems that undergo movement after shutdown.

In Chapter 3, the TR2S method for calculating the SDR in systems that move after shutdown was introduced. It was shown that performing the TR2S method can give insight into the dose rate along the proposed path of movement of activated components and the dose that accumulates in the facility over time. This information can be beneficial in maintenance planning when determining the how soon after

shutdown the component can move and the best path around the facility for limiting the dose to sensitive regions. The number of time-steps simulated will be decided by the user based on problem-specific variables and ultimately needs to capture the features of the path that cause significant contributions to the SDR. In the future, an experiment with a moving, non-activation radiation source could be performed to validate this method.

In Chapter 5, the TGT-CADIS adjoint neutron source was derived and the implementation of the VR method was described. TGT-CADIS was then applied to a simple problem and compared to simulations run in analog and using FW-CADIS for optimization. It was found that the TGT-CADIS method efficiently reduces error in the regions that are most important to the final SDR. Future work is needed to determine the significance of the under-sampling in certain regions of the problem that are less important to the SDR and the cause of the single high-error element found in this experiment.

In Chapter 6, the TR2S and TGT-CADIS methods were applied to a production-level problem. The TGT-CADIS method produced VR parameters that when compared to analog, reduced the error in the neutron flux in the experimental port, an important contributor to the detector SDR. The TR2S method was then used to produce time-dependent SDR maps which are useful in visualizing how the SDR changes over the course of movement.

Accurately quantifying the SDR is a crucial step in the design and operation of FES in order to ensure that the facility is built and maintenance activities are planned in a manner that ensures the safety of plant personnel. The TR2S method can be used to explore the SDR over the time of geometry movement and the TGT-CADIS method provides the capabilities to reduce the error in simulations that involve activated components moving around a facility.

Appendix A

Appendix: Implementation Details

A.1 Efficient OBB Tree Generation

DAGMC facilitates radiation transport directly on CAD geometries [19]. The surfaces of the CAD geometry are discretized into a triangular mesh and stored within MOAB [20]. Particle tracking occurs on the faceted representation of the geometry.

One of the techniques used to accelerate a geometry query search over triangles is the Oriented Bounding Box (OBB) Bounding Volume Hierarchy (BVH). In essence, the triangles are divided geometrically into subsets and bound by OBBs. The triangles are divided into smaller and smaller subsets until there is a single box per triangle. The OBBs are stored in a hierarchical manner. Ray fire interesections occur at the OBBs instead of individual triangles allowing for fast elimination of sets of triangles from the search until the exact triangle for intersection is found [19]. Generating the OBB BVH can be time consuming, especially for large models.

In the case of moving geometries, it is possible that a single component moves and the rest of the geometry is static. Typically, the OBB tree is built at transport runtime. When performing step-wise simulations that involve partial geometry

movement, it is wasteful to regenerate the entire OBB tree for every time-step. This is remedied by the geometry transformation script; the full OBB tree for the original configuration is built once and only the OBB trees for the component(s) that move and the OBB tree for the implicit complement are regenerated at each time step. At runtime, the OBB tree is loaded from the geometry file instead of being built from scratch.

A.2 Mesh Mapping

The TGT-CADIS method involves radiation transport with mesh-based sources on mesh-based geometries. Both neutron and photon adjoint transport is performed deterministically and the sources and results are defined on a global, structured (Cartesian) mesh. Monte Carlo transport is performed on CAD-based geometries and the sources and results are defined on either conformal or global, unstructured (tetrahedral) meshes. Because parts of this workflow involve combining results from different meshes, it is necessary to map the results from one mesh onto another.

A script was created to map any tagged result (e.g. flux, error, source density, etc.) from a donor mesh onto a receiver mesh. It operates by looping over every mesh element in the receiver, calculating its centroid, finding the mesh element of the donor that encapsulates the centroid, and copying the tagged result to the receiver. This process is most successful when the sizes of mesh elements are very similar.

Bibliography

[1] Y Chen and U Fischer. Rigorous MCNP based shutdown dose rate calculations: computational scheme, verification calculations and application to ITER. *Fusion Engineering and Design*, 63:107 – 114, 2002.

[2] Ahmad M. Ibrahim, Douglas E. Peplow, Robert E. Grove, Joshua L. Peterson, and Seth R. Johnson. The Multi-Step CADIS method for shutdown dose rate calclulations and uncertainty propagation. *Nuclear Technology*, 192:286 – 298, 2015.

[3] Elliott D. Biondo and Paul P. H. Wilson. Transmutation approximations for the application of hybrid Monte Carlo/deterministic neutron transport to shutdown dose rate analysis. *Nuclear Science and Engineering*, 187(1):27–48, 2017.

[4] Elmer Lewis and Warren Miller. *Computational Methods of Neutron Transport*. American Nuclear Society, Inc., 1993.

[5] X-5 Monte Carlo Team. *MCNP- A General Monte Carlo N-Particle Transport Code, Version 5*. April 2003.

[6] Davide Valenza, Hiromasa Iida, Romano Plenteda, and Robert T. Santoro. Proposal of shutdown dose estimation method by Monte Carlo code. *Fusion Engineering and Design*, 55(4):411 – 418, 2001.

[7] R. Forrest. Fispact-2007: User manual. *Easy Documentation Series*, UKAEA FUS 534.

[8] Rosaria Villari and Luigino Petrizzi Davide Flammini, Fabio Moro. Development of the advanced D1S for shutdown dose rate calculations in fusion reactors. *Transactions of the American Nuclear Society*, 116:255–258, 2017.

[9] A. Davis and R. Pampin. Benchmarking the MCR2S system for high-resolution activation dose analysis in ITER. *Fusion Engineering and Design*, 85(1):87 – 92, 2010.

[10] Cameron Bates, Elliott Biondo, and Kathryn Huff. PyNE progress report. 11 2014.

[11] Elliott D. Biondo, Andrew Davis, and Paul P.H. Wilson. Shutdown dose rate analysis with CAD geometry, Cartesian/tetrahedral mesh, and advanced variance reduction. *Fusion Engineering and Design*, 106(Supplement C):77 – 84, 2016.

[12] Paul Wilson, H Tsige-Tamirat, Hesham Khater, and Douglass Henderson. Validation of the ALARA activation code. 34:784, 01 1998.

[13] Alireza Haghighat and John C. Wagner. Monte Carlo Variance Reduction with Deterministic Importance Functions. *Progress in Nuclear Energy*, 42(1):25–53, 2003.

[14] L.L. Carter and E.D. Cashwell. *Particle-transport Simulation with the Monte Carlo Method*. Jan 1975.

[15] John C. Wagner, Douglas E. Peplow, and Scott W. Mosher. FW-CADIS method for global and regional variance reduction of Monte Carlo radiation transport calculations. *Nuclear Science and Engineering*, 176(1):37–57, 2014.

[16] Joe W. Durkee, Russell C. Johns, and Laurie S. Waters. MCNP6 moving objects part I: Theory. *Progress in Nuclear Energy*, 87(Supplement C):104 – 121, 2016.

[17] Joe W. Durkee, Russell C. Johns, and Laurie S. Waters. MCNP6 moving objects. part ii: Simulations. *Progress in Nuclear Energy*, 87(Supplement C):122 – 143, 2016.

[18] Tim Eade, Steven Lilley, Zamir Ghani, and Etienne Delmas. Movement of active components in the shutdown dose rate analysis of the ITER neutral beam injectors. *Fusion Engineering and Design*, 98-99(Supplement C):2130 – 2133, 2015. Proceedings of the 28th Symposium On Fusion Technology (SOFT-28).

[19] Timothy Tautges, Paul Wilson, Jason Kraftcheck, Brandon F Smith, and Douglass Henderson. Acceleration techniques for direct use of CAD-based geometries in Monte Carlo radiation transport. may 2009.

[20] Timothy J. Tautges, R. Meyers, K. Merkley, C. Stimpson, and C. Ernst. MOAB: A Mesh-Oriented Database, 2004.

[21] Sandia National Laboratories. Trelis 16.4 User Documentation: Advanced Meshing for Challenging Simulations, 2013-2017.

[22] E. Sartori and G. Panini. ZZ Groupstructures, VITAMIN-J, XMAS, ECCO-33, ECCO2000 Standard Group Structures. Tech. Rep. 40-03, 1991.

[23] A.B. Pashchenko and H. Wienke. The processed FENDL-2 neutron activation cross-section data files summary documentation. *www-nds.iaea.org*, 1997.

[24] R. Alcouffe, R. Baker, J. Dahl, S. Turner, and R. Ward. PARTISN: A time-dependent, parallel neutral particle transport code system. (LA-UR-05-3925), May 2005.

[25] ICRP. Conversion coefficients for use in radiological protection against external radiation. *ICRP Publication 74. Ann. ICRP*, 26:3–4.

[26] Oak Ridge National Laboratory. *ADVANTG 3.0.3: AutomateD VAriaNce reduc-Tion Generator, 3.0.3 ed.*, 2015.

[27] Elliott Biondo. Hybrid Monte Carlo/Deterministic Neutron Transport for Shutdown Dose Rate Analysis of Fusion Energy Systems. *Preliminary Exam*, July 2015.

[28] Elliott Biondo. Hybrid Monte Carlo/Deterministic Neutron Transport for Shutdown Dose Rate Analysis. *Dissertation*, July 2016.

[29] Moataz Harb. Propagation of Statistical Uncertainty in Mesh-Based Shutdown Dose Rate Calculations. *Preliminary Exam*, December 2017.

[30] Peng Lu, Ulrich Fischer, Pavel Pereslavtsev, Jiangang Li, and Yunato Song. Hybrid Monte Carlo approach for accurate and efficient shutdown dose rate calculation. In *13th International Symposium on Fusion Nuclear Technology*, 2017.